Geochemistry, Geophysics, Geosystems®

RESEARCH ARTICLE
10.1029/2020GC009560

Insights Into the Nature of Plume-Ridge Interaction and Outflux of H_2O From the Galápagos Spreading Center

Matthew L. M. Gleeson[1,2] **and Sally A. Gibson**[1]

[1]Deparment of Earth Sciences, University of Cambridge, Cambridge, UK, [2]School of Earth and Environmental Sciences, Cardiff University, Cardiff, UK

Key Points:

- Basalts erupted on segments of the global ridge system adjacent to the Galapagos mantle plume have high volatile (H_2O and F) contents
- Channelized melt transport between the Galápagos mantle plume stem and the Galápagos Spreading Center (GSC) causes variations in crustal thickness and geochemistry
- Plume-derived volatile-rich melts contribute up to 20%–60% of the total H_2O outflux at the GSC

Supporting Information:

Supporting Information may be found in the online version of this article.

Correspondence to:

M. L. M. Gleeson,
gleesonm1@cardiff.ac.uk

Citation:

Gleeson, M. L. M., & Gibson, S. A. (2021). Insights into the nature of plume-ridge interaction and outflux of H_2O from the Galápagos Spreading Center. *Geochemistry, Geophysics, Geosystems*, *22*, e2020GC009560. https://doi.org/10.1029/2020GC009560

Received 20 NOV 2020
Accepted 18 OCT 2021

Author Contributions:

Conceptualization: Matthew L. M. Gleeson, Sally A. Gibson
Data curation: Matthew L. M. Gleeson
Formal analysis: Matthew L. M. Gleeson
Funding acquisition: Matthew L. M. Gleeson, Sally A. Gibson
Investigation: Matthew L. M. Gleeson
Methodology: Matthew L. M. Gleeson
Project Administration: Matthew L. M. Gleeson
Resources: Sally A. Gibson
Software: Matthew L. M. Gleeson
Supervision: Sally A. Gibson

Abstract The flow of high-temperature and compositionally enriched material between mantle plumes and nearby spreading centers influences up to 30% of the global mid-ocean ridge system and represents a significant, but currently unconstrained, flux of volatiles out of the mantle. Here, we present new analyses of H_2O, F, Cl, and S in basaltic glass chips from an archetypal region of plume-ridge interaction, the Galápagos Spreading Center (GSC). Our data set includes samples from the eastern GSC, on ridge segments that are strongly influenced by the adjacent Galápagos mantle plume, and complements published analyses of volatiles largely from the western GSC. We use forward models of mantle melting to investigate the role of solid and melt-phase transport from a lithologically heterogeneous (peridotite-pyroxenite) mantle in plume-ridge interaction along approximately 1,000 km of the GSC. Our results indicate that the observed geochemical and geophysical variations cannot be recreated by models that only involve solid-state transfer of material between the Galápagos mantle plume and the GSC. Instead, we show that the geochemical and geophysical data from the GSC are well-matched by models that incorporate channelized flow of volatile-rich melts formed at high-pressures (>3 GPa) in the Galápagos plume stem to the GSC. In addition, our new models demonstrate that channelized flow of enriched, plume-derived melt can account for up to ~60% of the H_2O outgassed from regions of the GSC, which are most strongly influenced by the Galápagos mantle plume.

Plain Language Summary Approximately one-third of Earth's global mid-ocean ridge system is influenced by the transfer of compositionally distinct material from nearby upwellings of anomalously hot mantle. Transfer of this plume material to oceanic spreading centers might represent an important mechanism of volatile loss from Earth's mantle, but there are limited constraints on the quantities of H_2O and other volatiles that degas from these plume-influenced spreading centers. In this study, we evaluate the mechanism of plume-ridge interaction between the Galápagos mantle plume and the nearby Galápagos Spreading Center (GSC) using new analyses of volatiles in basalts erupted on the ridge. The results from new numerical models demonstrate that the geochemical and geophysical signatures of plume-ridge interaction along the GSC are best explained if the transport of deep sourced mantle material between the Galápagos mantle plume and GSC occurs in the melt phase rather than as a solid. In addition, our new analyses enable us to constrain the flux of H_2O out of the GSC and demonstrate that melt channelization can account for up to ~60% of the H_2O flux out of plume-influenced ridges.

1. Introduction

The majority of ocean island basalts (OIBs) are believed to form as a consequence of adiabatic decompression melting in high-temperature, and potentially lithologically heterogeneous, mantle plumes (Asimow & Langmuir, 2003; Herzberg & Asimow, 2008; Ito & Mahoney, 2005; Métrich et al., 2014; Morgan, 1971; Sobolev et al., 2007). Higher concentrations of volatiles (such as H_2O, F, or Cl) in OIBs compared to mid-ocean ridge basalts (MORBs) reflect the volatile-rich nature of deep-sourced plume material, relative to the MORB source, and are evidence of small-fraction decompression melting at higher pressures than the anhydrous peridotite solidus (Dixon et al., 2017; Gibson & Richards, 2018; Ingle et al., 2010; Jackson et al., 2015; Koleszar et al., 2009; Métrich et al., 2014). In addition, approximately 30% of the global mid-ocean ridge (MOR) system is influenced by the lateral transfer of deep-sourced mantle plume material (Ito & Lin, 1995) and potentially represent sites of substantial volatile outgassing from the Earth's mantle (Gibson & Richards, 2018; Le Voyer et al., 2018). Nevertheless, robust estimates for the outflux of volatiles from mantle plume influenced segments of MORs are rare. In addition, there remain outstanding issues related

Writing – original draft: Matthew L. M. Gleeson
Writing – review & editing: Matthew L. M. Gleeson, Sally A. Gibson

to the role of melt channelization in the transfer of geochemically enriched plume material between mantle plume stems and nearby spreading centers.

Over the past few decades, numerous hypotheses have been put forward to explain both the long and short length-scale geochemical and geophysical heterogeneities that are observed along plume-influenced regions of the global MOR system. These previously proposed hypotheses include: (a) buoyancy-driven upwelling of solid peridotite beneath ridge segments that are most strongly influenced by nearby mantle plumes (e.g., Ingle et al., 2010; Maclennan et al., 2001; Sleep, 1990); (b) radial spreading of solid plume material, consisting of enriched blebs embedded in a depleted matrix (and the role of these enriched components in dynamic plume flow; Bianco et al., 2013; Ito & Bianco, 2014; Ito & Mahoney, 2005; Ribe, 1996; Shorttle et al., 2010); (c) flow of solid plume material in a sub-lithospheric channel (Morgan, 1978; Schilling et al., 1982); (d) melt transport via porous flow at the base of the lithosphere (Braun & Sohn, 2003); and (e) channelized buoyancy-driven flow of off-axis plume-derived melts in a matrix of dispersing solid plume material (Gibson et al., 2015; Gibson & Richards, 2018; Mittal & Richards, 2017; Stroncik & Devey, 2011; Stroncik et al., 2008).

Channelized, buoyancy-driven flow of volatile-rich melts in a network of channels embedded in a spreading "puddle" of solid plume material (hypothesis (v) above) was first put forward by Gibson et al. (2015) to account for the simultaneous presence of enriched basalts on the GSC and depleted basalts found in nearby regions of the northeast Galápagos Archipelago (e.g., Genovesa). Subsequently, Mittal and Richards (2017) and Gibson and Richards (2018) extended this conceptual model to account for certain enigmatic features at global sites of plume-ridge interaction (including the Galápagos, the Azores, Discovery, and Reunion), such as the coincidence of the intersection of non-age progressive volcanic lineaments with excess crustal thickness and short length-scale geochemical anomalies (i.e., highly enriched basalts) on the spreading ridge.

Despite continued development in the conceptual models of plume-ridge interaction via a network of melt channels embedded in solid plume material, a focused geochemical study on the role of channelized volatile-rich melts to an individual spreading center has yet to be undertaken. Here, we present new volatile data (H_2O, F, Cl, and S) for basaltic glass chips from plume-influenced segments of the GSC, including the eastern GSC where only limited volatile data previously existed (e.g., Byers et al., 1983). We use our new and published volatile data in combination with forward melting models to evaluate whether plume-ridge interaction via channelized flow of volatile-rich melts derived from a pyroxenitic source component in a mixed peridotite-pyroxenite mantle can explain the long (100s of km) and short (10s of km) length-scale heterogeneities observed in basalt chemistry and crustal thickness at this single site of plume-ridge interaction. Our new volatile data and forward models of mantle melting also allow us to estimate the outflux of H_2O from the entire region of Galápagos plume-influenced ridge.

2. Geological Background

2.1. Mantle Heterogeneity

Located ~1,000 km off the western coast of Ecuador, the Galápagos Archipelago represents a well-known example of mantle plume related volcanism (Morgan, 1978). Active and recent Holocene volcanism is observed over a wide geographic area and geochemical studies of both subaerial and submarine basaltic lavas reveal that compositional heterogeneity results from the melting of at least four isotopically distinct components in the Galápagos mantle plume (Geist et al., 1998; Harpp & Weis, 2020; Harpp & White, 2001; Hoernle et al., 2000; White et al., 1993; White & Hofmann, 1978). The isotopic end-members of the Galápagos mantle plume include an isotopically depleted component and three isotopically enriched mantle components, that can be summarized as:

1. PLUME component—dominant in basalts from the western Galápagos Archipelago (centered on Isla Fernandina), which are characterized by moderately enriched Sr, Nd, and Pb isotope ratios and elevated $^3He/^4He$ ratios (~30 R/R_A; Harpp & White, 2001; Kurz et al., 2009; Kurz & Geist, 1999). The isotopic signatures of the PLUME component resembles the "FOZO" or "C" global mantle end-member (Hanan & Graham, 1996; Hart et al., 1992).
2. Floreana (FLO) component—centered on the southern island of Floreana and characterized by the most radiogenic Sr and Pb isotope signatures observed anywhere in the Galápagos (Harpp, Geist, et al., 2014;

Harpp & White, 2001). The FLO component is hypothesized to result from melting of ancient recycled oceanic crust (~2.2–2.5 Ga) incorporated into the Galápagos plume (Gibson et al., 2016; Harpp, Geist, et al., 2014).

3. Wolf–Darwin (WD) component—most prevalent in basaltic lavas from the northern islands of Pinta, Wolf, Darwin, and surrounding seamounts (Harpp, Wirth, et al., 2014; Harpp & White, 2001). The WD component is characterized by elevated $^{208}Pb/^{206}Pb$ and $^{207}Pb/^{206}Pb$ ratios (Harpp & White, 2001). The origin of this component remains enigmatic.

The spatial heterogeneity in the radiogenic isotope composition of basalts erupted in the Galápagos Archipelago provides insights into the structure of the underlying plume and the deep mantle. For example, isotopically enriched signatures are most commonly observed in the south-western Archipelago (corresponding to the PLUME and FLO components), whereas isotopically depleted basalts are typically found further east (Harpp & Weis, 2020; Harpp & White, 2001; Hoernle et al., 2000; White et al., 1993; White & Hofmann, 1978). This bilateral asymmetry in the composition of the upwelling mantle plume, which is similar to that observed in Hawaii and other regions of plume-derived volcanism worldwide (Harpp, Hall, & Jackson, 2014; Weis et al., 2011), has been linked to the presence of deep mantle superstructures at the base of the Galápagos plume (Gleeson et al., 2021; Harpp & Weis, 2020). Specifically, the isotopically enriched signatures of the south-western Galápagos have been assigned to melting of material originating in the Pacific Large Low Shear Velocity Province, while the isotopically depleted signatures of the eastern Galápagos volcanoes are assigned to melting of the ambient Pacific lower mantle or entrained upper mantle material (Harpp & Weis, 2020). This simple picture of mantle isotopic heterogeneity in the Galápagos plume is complicated by the non-trivial relationship between isotopic and lithological heterogeneity. Olivine minor element concentrations were originally used to indicate that both isotopically enriched and isotopically depleted pyroxenite components are present in the Galápagos mantle plume (Vidito et al., 2013). However, recent models that consider the influence of magma chamber recharge on the minor element contents of magmatic olivines suggest that basalts sourced from the isotopically depleted mantle component in the Galápagos plume are predominantly derived from a peridotitic source (Gleeson & Gibson, 2019). Nevertheless, variations in the Fe-isotope composition of the GSC basalts indicate that both peridotite and pyroxenite source components might contribute to the composition of plume-influenced basalts on the GSC (Gleeson et al., 2020, 2021).

2.2. Geophysical and Geochemical Heterogeneity Along the GSC

The Galápagos Spreading Center (GSC) separates the Cocos and Nazca tectonic plates and lies ~150–250 km north of the center of Galápagos plume upwelling, at 100 km depth, that has been postulated from seismic tomography (Figure 1; Hooft et al., 2003; Villagómez et al., 2014). This lies to the north-east of the postulated location of the plume stem at 200 km depth, that is, beneath southern Isabela. Variations in crustal thickness and ridge morphology provide evidence for the influence of the Galápagos mantle plume along a ~1,000 km wide zone of the GSC, extending between 85.5° and 95.5°W (e.g., Christie et al., 2005; Ito & Lin, 1995). For example, a crustal thickness high is observed at ~90.5°W, near the closest point on the GSC to the center of the mantle plume upwelling (Canales et al., 2002; Christie et al., 2005; Detrick et al., 2002; Mittelstaedt et al., 2014).

Several features observed along both the eastern and western GSC, which are separated by a major transform fault at ~91°W (the Galápagos Transform fault—GTF; Figure 1), are consistent with a decrease in magma supply with increasing distance from the mantle plume (Canales et al., 2014). For example, changes in ridge morphology, from a low-relief valley and ridge terrain to a prominent axial ridge, are observed on both ridge segments as the separation distance between the ridge and hotspot decreases (Christie et al., 2005; Sinton et al., 2003). In addition, along the western GSC the depth of the seismically-imaged magma lens increases from 1 to 2.5 km east of 92.5°W to 2.5–4.5 km between 92.7 and 94.7°W, corresponding to a change from fissure-fed eruptions near the GTF to point source eruptions further west (Behn et al., 2004; Blacic et al., 2004).

A prominent geochemical anomaly has been observed on the GSC near the GTF, between 89.5 and 92.5°W (Christie et al., 2005; Ingle et al., 2010; Schilling et al., 2003). Basalts erupted within this region

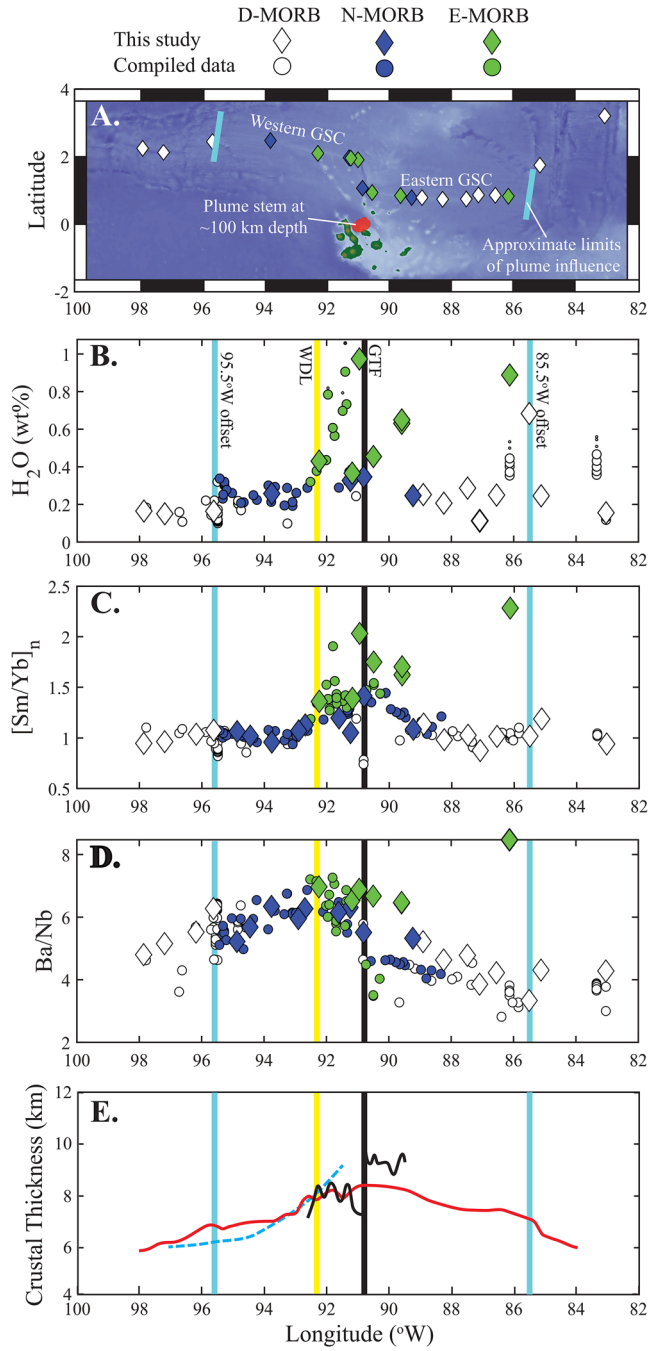

Figure 1. Location and chemistry of the basalts from the GSC. (a) Map of the Galápagos Spreading Center (GSC) and Galápagos Archipelago (bathymetric data from Ryan et al., 2009). (b) Brine-assimilation corrected H_2O contents in the GSC basalts from this study (diamonds) and from Cushman et al. (2004) and Le Voyer et al. (2018; circles). The measured H_2O contents of these basalts are shown by the small dots (only visible where large differences between the measured and corrected H_2O concentrations are seen; Supporting Information S1). Panels (c) and (d) show key trace element ratios ($[Sm/Yb]_n$ and Ba/Nb, respectively), which display an increased contribution from melts of a garnet-bearing lithology near the Galápagos Transform Fault (GTF) (c); and a geochemical offset between the western and eastern GSC, which relates to the incorporation of the Wolf-Darwin component in the mantle beneath the western GSC (d) (data from Christie et al., 2005; Gleeson et al., 2020; Ingle et al., 2010). Crustal thickness estimates are shown in panel (e) from Ito and Lin (1995; red), Canales et al. (2002; blue), and Mittelstaedt et al. (2014; black). 2σ error is smaller than the symbol size for all graphs. Yellow line represents the intersection of the Wolf-Darwin Lineament with the GSC. The blue lines represent the approximate limit of plume influence along the GSC.

are characterized by elevated concentrations of strongly incompatible trace elements (e.g., Nb, La) together with radiogenic Sr and Pb and unradiogenic Nd and Hf isotope ratios (Christie et al., 2005; Gleeson et al., 2020; Ingle et al., 2010; Schilling et al., 1982, 2003). Many incompatible trace element ratios (such as Sm/Yb and Nb/Zr) display broadly symmetric profiles that are centered around ~91–91.5°W, just to the west of the GTF (Figure 1). In addition, positive correlations between the large variations in incompatible trace element enrichment and Fe-isotopes in the GSC basalts imply that the plume-influenced GSC basalts may be formed through melting of a lithologically heterogeneous mantle source (Gleeson et al., 2020).

Some important differences exist between the eastern and the western GSC. First, the highest resolution gravity and multi-beam bathymetry data available indicates that crustal thickness increases by ~1 km from west to east across the GTF (Mittelstaedt et al., 2014). Second, the eastern GSC basalts generally have lower ratios of fluid-mobile to fluid-immobile trace elements (e.g., Ba/Nb; Figure 1) and lower $^{208}Pb/^{204}Pb$ and $^{207}Pb/^{204}Pb$ ratios than basalts from the western GSC (e.g., Christie et al., 2005; Gibson et al., 2015; Ingle et al., 2010; Schilling et al., 2003). The long length-scale east-to-west geochemical differences on the GSC have been attributed to an additional contribution of melts from the isotopically enriched WD Galápagos mantle component beneath the western GSC (Gibson et al., 2015; Ingle et al., 2010; Schilling et al., 2003).

Gibson and Richards (2018) observed a series of short length-scale geochemical and geophysical features that are superimposed on the broad length-scale heterogeneity of the GSC. For example, basalts with anomalously high H_2O contents relative to their neighboring basalts (typically >0.4 wt.%), and short length-scale crustal thickness anomalies occur at locations where long-lived volcanic lineaments intersect the GSC (Mittelstaedt et al., 2014; Sinton et al., 2003). As a result, it has been suggested that melt channels embedded within the "normal" spreading of Galápagos plume material may represent an important component of plume-ridge interaction (Gibson & Richards, 2018; Mittal & Richards, 2017). In this study, we use new melting models to critically evaluate the role of both a mixed peridotite-pyroxenite mantle and melt channelization from the Galápagos plume stem in generating short and long length-scale geochemical and geophysical heterogeneities on the GSC. In addition, our new data expands the existing volatile data set for the GSC and enables us to place improved constraints on the flux of H_2O out of the entire segment of plume-influenced ridge.

3. Methodology

Twenty-two chips of basaltic glass (1–10 mm diameter) collected between 83° and 98°W on the GSC were selected from the Jean-Guy Schilling collection at the University of Rhode Island, USA. Here we present new analyses of their H_2O, F, Cl, and S concentrations (Figure 1). The major and trace element contents of the selected glasses, together with their Fe, Sr, Nd, Hf, and Pb isotope ratios, have previously been reported (Gleeson et al., 2020; Schilling et al., 2003). We primarily selected samples from the eastern GSC for this analysis, as only limited volatile data previously existed in this region, but a small number of samples ($n = 6$) were chosen from the western GSC to check that our results are consistent with previous studies (e.g., Cushman et al., 2004; Ingle et al., 2010).

Basaltic glass chips in polished epoxy mounts were analyzed for sulfur on a Cameca SX100 EPMA in the Department of Earth Sciences at the University of Cambridge. Sulfur was analyzed alongside major elements (following methods described in Gleeson et al., 2020) to calculate the required matrix correction. The S concentrations were determined by counting for 90 s on the K_a peak using a beam current of 10 nA, an acceleration voltage of 15 kV, and a defocussed beam (10 μm). Data quality was checked using the VG2 basaltic glass standard (Jarosewich et al., 1980).

Prior to analysis of H_2O, F, and Cl on a Cameca ims-4f at the NERC Edinburgh Ion Microprobe Facility (EIMF), the GSC glasses were briefly re-ground and polished, to remove topography caused by prior laser ablation analysis, and gold coated. Secondary Ion Mass Spectrometry (SIMS) analysis was carried out using a $^{16}O^-$ primary ion beam and a 14.5 keV net impact energy (4.5 keV secondary ion accelerating voltage). A liquid nitrogen cold trap was used to reduce background counts on volatile elements during analysis. Both static and electrostatic magnets were applied to center H^+ ion images relative to heavier masses. A 3 min, 20 μm square raster pre-sputter was applied to reduce H^+ background. Analysis was then carried out using

a 15–20 μm spot. Secondary ions were analyzed with a 25 μm image field. Analysis of quartz crystals at regular intervals during analysis was used to determine H^+ backgrounds (<0.02 wt%).

The SIMS data were collected over eight cycles with total count times of 30 s for ^{1}H and 80 s for ^{19}F, 40 s for ^{35}Cl, and 16 s for ^{30}Si, which was used for internal standardization. ^{1}H counts were only recorded for the final six cycles to avoid any contamination. H_2O concentrations for the GSC glasses were calculated using a H_2O versus $^{1}H/^{30}Si$ calibration slope determined using analyses of BCR-2g (anhydrous) and standards St-1, St-2, and St-6 from Shishkina et al. (2010). Calibration slopes for F and Cl (F vs. $^{19}F/^{30}Si \times SiO_2$ and Cl vs. $^{35}Cl/^{30}Si \times SiO_2$) were determined using the composition of BCR-2g from Marks et al. (2017). The 2σ analytical precision for H_2O (3.5%), F (8%), and Cl (16%) was constrained using five repeat measurements of GSC basalt TR164 11D-1g.

4. Results

Our new SIMS and EPMA data represent the first systematic analyses of H_2O, F, S, and Cl for well-characterized D-, N-, and E-MORB erupted on the eastern GSC (geochemical divisions are the same as those used in Gleeson et al., 2020) and, thus, expand the published volatile data set to cover the entire section of the Galápagos plume-influenced ridge (Cushman et al., 2004; Ingle et al., 2010; Le Voyer et al., 2018; Michael, 1995).

4.1. Degassing, Contamination, and Fractional Crystallisation

The volatile contents of oceanic basalts are highly susceptible to modification by degassing, contamination and crystal fractionation (Dixon, 1997; Kendrick et al., 2015; Workman et al., 2006). All of the GSC samples analyzed in this study were collected at water depths >1,500 m and erupted under high enough pressure to minimize loss of H_2O to a vapor phase (Dixon, 1997; Iacovino et al., 2020; Shishkina et al., 2014). As a result, we estimate that degassing had only a minor influence on the H_2O content of these GSC basalts (generally <2% loss; see Supporting Information S1).

An indication of the extent of magmatic interaction with seawater or hydrothermal brines, which can substantially influence the H_2O contents measured in submarine basalts (Kendrick et al., 2015), is provided by the Cl and K_2O concentrations of basaltic lavas. In the GSC basalts, Cl exhibits a large range (9–3,360 ppm) and almost all samples have Cl/K ratios that are much greater than those previously proposed for primary OIBs or MORBs (Figure 2a; 0.01–0.08, with some regions up to 0.15; Kendrick et al., 2015; Le Roux et al., 2006; Michael & Cornell, 1998). We therefore suspect that GSC basalts have assimilated a Cl-rich component (i.e., a brine).

We used the H_2O/Cl, K/Cl, and F/Cl ratios of the GSC basalts, together with an assumed Cl/K ratio of 0.08, to evaluate and correct for the effects of brine assimilation on their H_2O contents (see Supporting Information S1). Owing to the influence of brine assimilation on the Cl content of the GSC basalts, we do not attempt to constrain variations in the Cl/K or Cl/Nb ratio of their mantle source regions. Likewise, although S is commonly hypothesized to behave similarly to Dy during mantle melting (Figure 2b; Peterson et al., 2017), recent studies have shown that concentrations of chalcophile elements (such as Se, Ag, and Cu) are required to truly evaluate the behavior of S during mantle melting and fractional crystallisation (Reekie et al., 2019; Sun et al., 2020; Wieser et al., 2020). Since chalcophile element data is not available for our samples, we focus on constraining only the H_2O and F systematics of the GSC mantle source regions.

To account for sub-ridge magma chamber processes, we have corrected the volatile data from the GSC basalts for fractional crystallisation (to 8 wt.% MgO), using the method outlined for major and trace elements by Gleeson et al. (2020) and mineral-melt volatile element partition coefficients published by Hauri et al. (2006) and Johnson (2006).

4.2. Variations in H_2O and F Contents of GSC Basalts

Our new SIMS data reveal that basalts from the GSC exhibit large variations in H_2O, with basalts from the western GSC reaching higher concentrations (0.10–1.08 wt.%; Cushman et al., 2004) than those on the

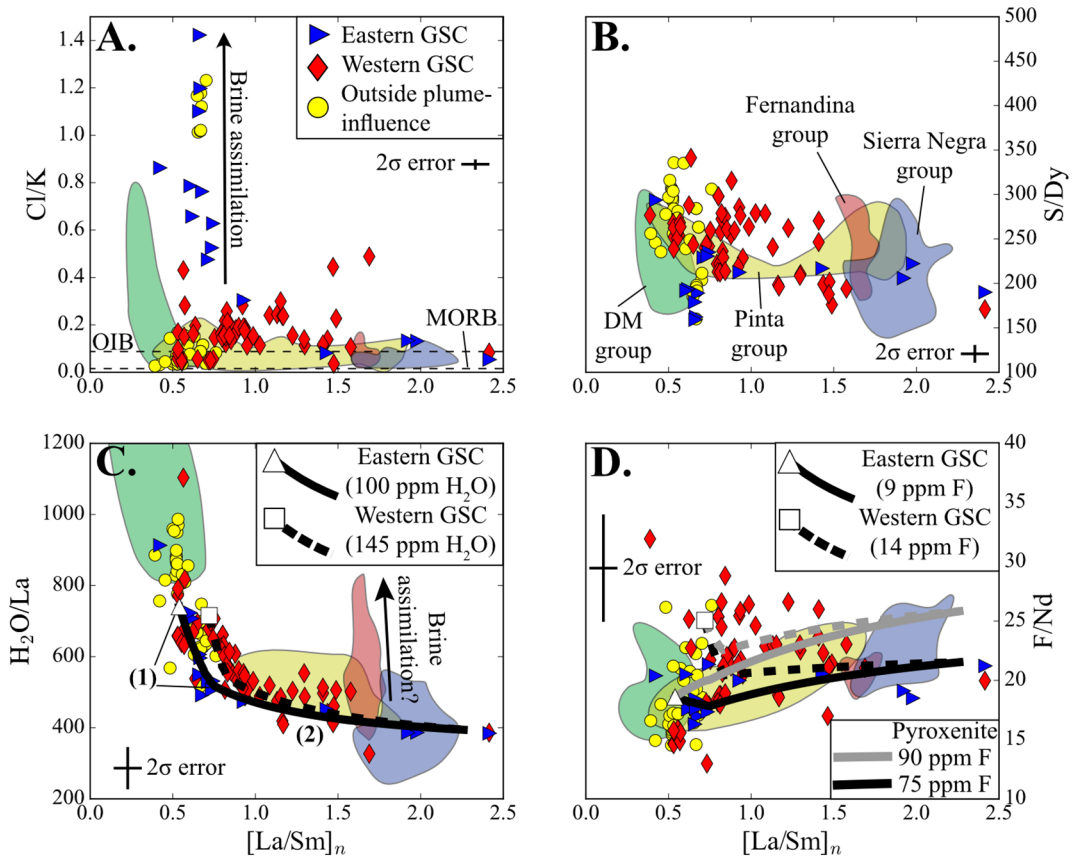

Figure 2. Relationship between volatile to non-volatile incompatible trace element ratios (e.g., H_2O/La) and indices of enrichment (represented here by $[La/Sm]_n$). Shown in *all* panels are the composition of the GSC basalts (color coded according to location) as well as the composition of submarine basalts from the Galápagos Archipelago measured by Peterson et al. (2017). (a) Many of the GSC basalts contain higher Cl/K ratios than those typically seen in MORBs or OIBs. Fernandina melt inclusions have Cl/K ratios of ~0.038 (Koleszar et al., 2009). (b) The S/Dy ratios of GSC basalts are similar to those observed in basaltic glass chips from across the archipelago (Peterson et al., 2017). (c) The H_2O/La ratio of plume-influenced GSC basalts varies from ~750 in depleted samples to <400 in the enriched samples. The white symbols and black lines show the compositions predicted by mantle melting models in this study. In the region labeled (1), the black lines display the influence of increasing the amount of pyroxenitic material in the mantle source beneath the GSC (up to 8%, consistent with the models shown in Figure 5). Region (2) displays the influence of increasing the contribution of channelized, plume-derived melts from a pyroxenitic source with ~550 ppm H_2O. The H_2O data from the GSC has been corrected for the influence of brine assimilation whereas the data for the submarine basalts from Peterson et al. (2017) has not (as different correction factors are required for each data set). (d) Black lines show the model predictions for increasing contribution of channelized flow where the enriched mantle end-member contains 75 ppm F. Gray lines show equivalent models for a scenario where the enriched, pyroxenitic end-member contains 90 ppm F. GSC data taken from this study (eastern GSC), Ingle et al. (2010), Cushman et al. (2004), and Le Voyer et al. (2018).

eastern GSC (0.12–0.87 wt.%); this is a significant difference given the relatively small analytical uncertainty of the H_2O analyses (predicted analytical error typically <<0.04 wt.%). Fluorine contents also show large variations in the GSC basalts; as with H_2O, F concentrations display a larger range in basalts from the western GSC (70–838 ppm; Ingle et al., 2010) compared to the eastern GSC (92–579 ppm). The highest concentrations of both H_2O (>0.4 wt.%) and F (>300 ppm) typically occur in basalts erupted between 89 and 92°W (i.e., on either side of the Galápagos Transform Fault, Figure 1), except for a single sample (ST7 17D-1g) collected from 86.13°W on the eastern GSC (bathymetry data show no evidence for a seamount or other topographic anomalies in this region; Ryan et al., 2009). Our new data collected from the western GSC displays comparable H_2O and F contents to similarly enriched samples previously analyzed by Ingle et al. (2010) and Cushman et al. (2004) and confirms that our analyses are consistent with those from previous studies.

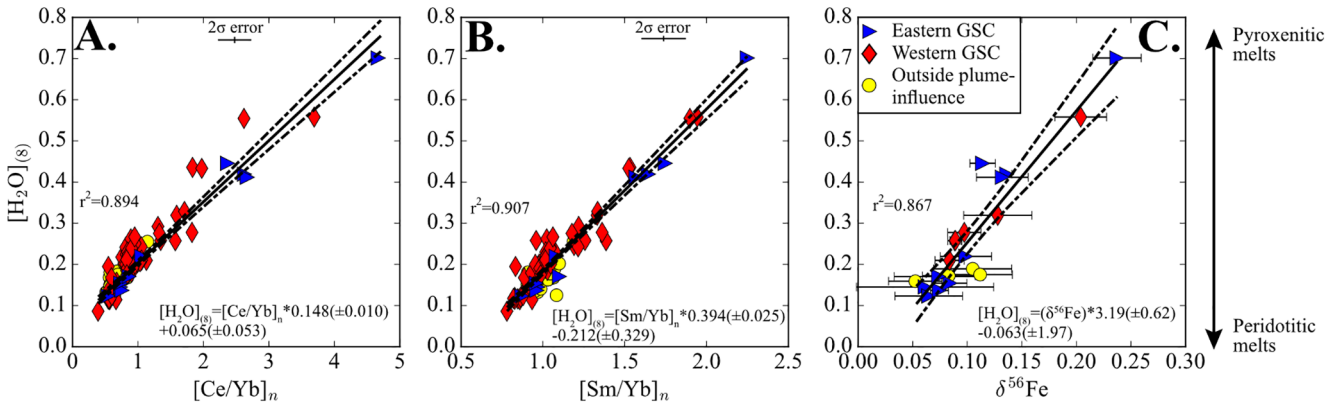

Figure 3. Relationship between $[H_2O]_{(8)}$ and key geochemical indices of compositional enrichment. (a and b) The correlation between trace element proxies of geochemical enrichment/melt fraction and $[H_2O]_{(8)}$ (fractionation corrected H_2O). The correlation between $[Sm/Yb]_n$ and $[H_2O]_{(8)}$ in panel (b) Is used to predict the fractionation corrected H_2O concentration of the GSC basalts for which volatile data does not exist. The data displayed here have been corrected for the influence of brine assimilation (Supporting Information S1). (c) A strong correlation is observed between $\delta^{56}Fe$ and $[H_2O]_{(8)}$, which indicates that there is a contribution of volatile-rich, pyroxenitic melts to the GSC basalts. Fe-isotope data from Gleeson et al. (2020), trace element and volatile element data from this study; Cushman et al. (2004), Gleeson et al. (2020), Ingle et al. (2010), and Le Voyer et al. (2018).

Both H_2O and F exhibit strong positive correlations with indices of trace element enrichment (such as $[La/Sm]_n$) in the GSC basalts (Figure 3; Supporting Information S1). Importantly, the GSC basalts with the highest H_2O and F contents (ST7 17D-1g and TR164 26D-3g) also have anomalously high $\delta^{56}Fe$ values (Gleeson et al., 2020, Figure 3). While Sr, Nd, or Pb isotope data are not available for ST7 17D-1g, we note that the volatile-rich sample TR164 26D-3g (90.95°W) has enriched $^{87}Sr/^{86}Sr$, $^{143}Nd/^{144}Nd$, and Pb isotopic ratios relative to other GSC basalts.

5. Constraining the Volatile Content of the GSC Mantle Source

A common method for determining the volatile concentrations in the mantle source region of oceanic basalts is to measure ratios of volatile and non-volatile trace elements that exhibit similar incompatibilities during melting and crystal fractionation (Cabral et al., 2014; Jackson et al., 2015; Koleszar et al., 2009; Michael, 1999; Saal et al., 2002). Widely used ratios include H_2O/La, H_2O/Ce, F/Nd, Cl/K, and S/Dy (Cabral et al., 2014; Jackson et al., 2015; Koleszar et al., 2009; Peterson et al., 2017; Saal et al., 2002), although others have been suggested (e.g., F/Zr; Le Voyer et al., 2015). In this study, we use the ratios H_2O/La and F/Nd to describe the volatile systematics of the different potential mantle components beneath the GSC (i.e., peridotite and pyroxenite). That is because, recent constraints from experiments at mantle conditions on the mineral-melt partitioning of H_2O and F (Dalou et al., 2012; Rosenthal et al., 2015), combined with new models of adiabatic decompression melting, indicate that H_2O displays similar compatibilities to La during melting of both peridotite and pyroxenite source components (see Supporting Information S1; H_2O partitioning data taken from Rosenthal et al., 2015). Fluorine is slightly less compatible than Nd during melting of a pyroxenitic source lithology and slightly more compatible during melting of a peridotitic source component (Supporting Information S1; F partitioning data taken from Dalou et al., 2012). These results are consistent with observations from global MORBs and OIBs (e.g., Danyushevsky et al., 2000; Kendrick et al., 2017).

The H_2O/La ratios of the GSC basalts exhibit a negative correlation with indices of geochemical enrichment (such as $[La/Sm]_n$; Figure 2c). Variations in the $[La/Sm]_n$ ratio of the GSC basalts could, theoretically, result from changes in the melt fraction of the mantle source; however, our mantle melting models indicate that the negative correlation between H_2O/La and $[La/Sm]_n$ is inconsistent with that predicted for melting of a single mantle source, as H_2O is slightly less compatible than La during large amounts of mantle melting (Supporting Information S1; Rosenthal et al., 2015). In addition, as the $[La/Sm]_n$ ratios of the GSC basalts have previously been shown to correlate with radiogenic and stable isotope ratios (Gleeson et al., 2020; Schilling et al., 2003), we suggest that the H_2O/La ratio of the GSC basalts is controlled by mixing of melts from multiple, lithologically distinct mantle components. Using the range of H_2O/La ratios measured in plume-influenced basalts from the GSC, we estimate that the peridotitic and enriched

(pyroxenitic) components in the mantle source region of the GSC basalts have H_2O/La ratios of ~750 and ~350–400, respectively (Figure 2). These estimates are supported by the results of our mantle melting models (see Supporting Information S1) utilizing recent experimentally determined mineral-melt partitioning data for H_2O (Figure 2; Rosenthal et al., 2015).

Unlike H_2O/La, the F/Nd ratio of the GSC basalts does not display a clear relationship with indices of geochemical enrichment (e.g., $[La/Sm]_n$; Figure 2d). The eastern GSC basalts have an average F/Nd ratio of 17.6 (±7.2; including literature data), which is slightly lower than the F/Nd ratio of the western GSC basalts (20.0 ± 7.3; Ingle et al., 2010). Notably, there is a large variation observed in the F/Nd ratios of D- and N-MORBs from the western GSC (potentially due to the poor counting statistics of EPMA analyses at low F concentrations; Ingle et al., 2010), with many of these basalts extending to substantially higher F/Nd ratios than that observed in submarine basaltic glasses and naturally quenched melt inclusions from the Galápagos Archipelago (Figure 2d; Koleszar et al., 2009; Peterson et al., 2017). Our new analyses for the eastern GSC basalts, however, reveal very similar F/Nd ratios to those analyzed from the Galápagos Platform (Figure 2d; Peterson et al., 2017).

To convert the H_2O/La and F/Nd ratios of the GSC basalts into mantle source volatile concentrations, knowledge of the trace element compositions of the different mantle components that contribute to the GSC basalts is required. In the modeling shown in Section 6, it is clear that the depleted composition (i.e., low $[La/Sm]_n$ ratios) of the plume-influenced D-MORBs from the eastern GSC can be reproduced by melting of a peridotitic component with the trace element composition of the depleted DMM (Depleted MORB Mantle; Workman & Hart, 2005). Therefore, if we assume the La concentration of the depleted peridotite component beneath the eastern GSC is ~0.134 ppm (Workman & Hart, 2005) and that this component is characterized by a H_2O/La ratio of ~750 (characteristic of the most-depleted plume-influenced GSC basalts), its H_2O concentration can be calculated to be ~100 ppm. Very similar estimates for the H_2O content of this component are obtained if H_2O/Ce is used in place of H_2O/La (~105 ppm H_2O; see Supporting Information S1). Our estimate for the H_2O content of the depleted peridotitic component beneath the GSC is slightly lower than the H_2O content estimated by Gibson and Richards (2018; 150 ppm) and similar to the estimates of Michael (1988), Saal et al. (2002), Salters and Stracke (2004), and Shimizu et al. (2016, 2019) for the depleted MORB source mantle.

The Pb-isotope compositions of basalts from the western GSC imply that they contain a small melt contribution from the enriched WD Galápagos mantle plume component (Gibson et al., 2015; Ingle et al., 2010). The H_2O content of the peridotitic mantle source beneath the western GSC, however, remains uncertain owing to the lack of constraints on the trace element composition of the WD component. Nevertheless, in the modeling shown below, we find that the trace element composition of N-MORBs located near the margin of plume influence along the western GSC, which are more enriched than basalts found at similar plume-ridge distances on the eastern GSC, can be produced by melting of moderately enriched mantle peridotite. We calculated this as a 90:10 mixture of the depleted DMM (Workman & Hart, 2005) and the enriched mantle component proposed by of Donnelly et al. (2004). Using this source composition, with a La content of 0.194, we estimate the H_2O content of the peridotitic mantle source beneath the western GSC is ~145 ppm (H_2O/La ~750). Importantly, models of mantle melting involving this hypothesized peridotitic component can reproduce both the trace element and H_2O contents of the western GSC N-MORBs located near 95.5°W (Figures 2 and 4).

Large uncertainties in the composition of recycled oceanic crust, and the relative contribution of ambient mantle peridotite and melts of a recycled crustal component to the formation of secondary pyroxenites, mean that the trace element and H_2O content of a pyroxenitic component are difficult to constrain. In our mantle melting models, we tested various potential solutions for the trace element composition of the pyroxenitic source that might contribute to the GSC basalts, and determined that a trace element composition similar to that proposed for the KG1 pyroxenite by Lambart (2017) can recreate the trace element systematics of the GSC basalts (Ce and Nd contents decreased by ~10% from the Lambart, 2017 estimate; Figures 4 and 5). Our estimated pyroxenitic source composition has a La content of ~1.415 ppm that, alongside an estimated H_2O/La ratio of ~350–400 for this source component, provides a H_2O estimate of 495–565 ppm. Our new data confirms that in the Galápagos mantle plume the enriched (pyroxenitic) component has a higher H_2O content than the isotopically depleted component (~100 ppm).

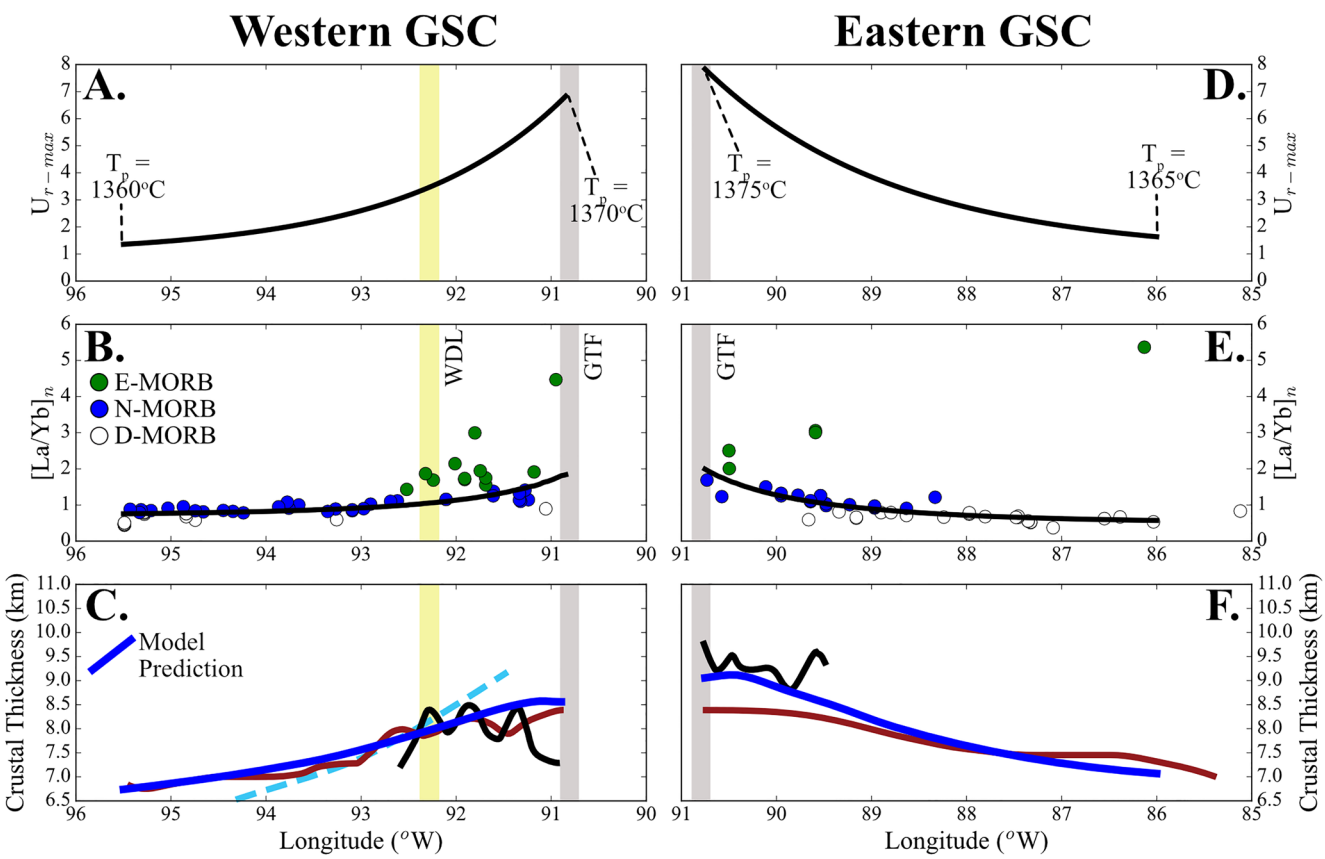

Figure 4. Results of plume-ridge interaction models that only account for solid-state transport between the Galápagos mantle plume and the GSC. Panels (a)–(c) show the results for the western GSC and panels (d)–(f) show the results for the eastern GSC. Panels (a) and (d) show the input parameters for these models, and the geochemical (b and e) and crustal thickness (c and f) results are shown below. Black lines in (b) and (e) display the mean composition of melts delivered to that section of ridge. Crustal thickness estimates are from Ito and Lin (1995; red), Canales et al. (2002; blue dashed), and Mittelstaedt et al. (2014; black); modeled crustal thickness is shown in blue (solid line). Some of the long length-scale trends in geochemical enrichment are reproduced along the GSC; however, several discrepancies can be observed between the model predictions and the crustal thickness and geochemical data from the GSC.

Our new estimates for the H_2O contents of the GSC peridotitic components are uninfluenced by the choice of ratio to describe the behavior of H_2O (i.e., H_2O/La or H_2O/Ce). However, the H_2O estimates derived from the enriched (pyroxenite) component are higher if we use the ratio H_2O/Ce (3.81 ppm Ce, H_2O/Ce ~170 and, therefore, H_2O ~650 ppm) rather than H_2O/La (H_2O ~495–565 ppm). However, we note that both the H_2O/La and H_2O/Ce contents of the GSC can be recreated by our mantle melting models when the pyroxenitic source component has a H_2O content around ~550 ppm (Figure 2c; Supporting Information S1).

If we assume that F acts comparably to Nd during mantle melting (which is consistent with some experimental data and the strong correlation between these elements in many MORB suites; Dalou et al., 2012; Kendrick et al., 2017), then, the F content of the depleted mantle component beneath the eastern GSC can be estimated from its Nd content (assumed to be ~0.48 ppm, equivalent to that of the depleted DMM; Workman & Hart, 2005) and the F/Nd ratio of the depleted eastern GSC basalts (~16–18). The results of these calculations give a F content of 7.7–8.7 ppm, the upper limit of which is shown to recreate the F/Nd systematics of the eastern GSC basalts in our forward models of mantle melting (Figure 2d).

Similarly, taking a source Nd concentration of ~0.56 ppm (calculated assuming a 90:10 mixture of depleted DMM and enriched mantle for the western GSC peridotite), we can constrain the F content of the peridotitic component beneath the western GSC to 8.4–15.6 ppm (assuming a characteristic F/Nd ratio of 15–30), consistent with the western GSC data (Ingle et al., 2010). Finally, if we take the F/Nd ratio of the most enriched GSC basalts (20–21.5) to be characteristic of the pyroxenitic mantle source component, the source F concentration is calculated to be 80–86 ppm (source Nd concentration of 4.00 ppm). However, our

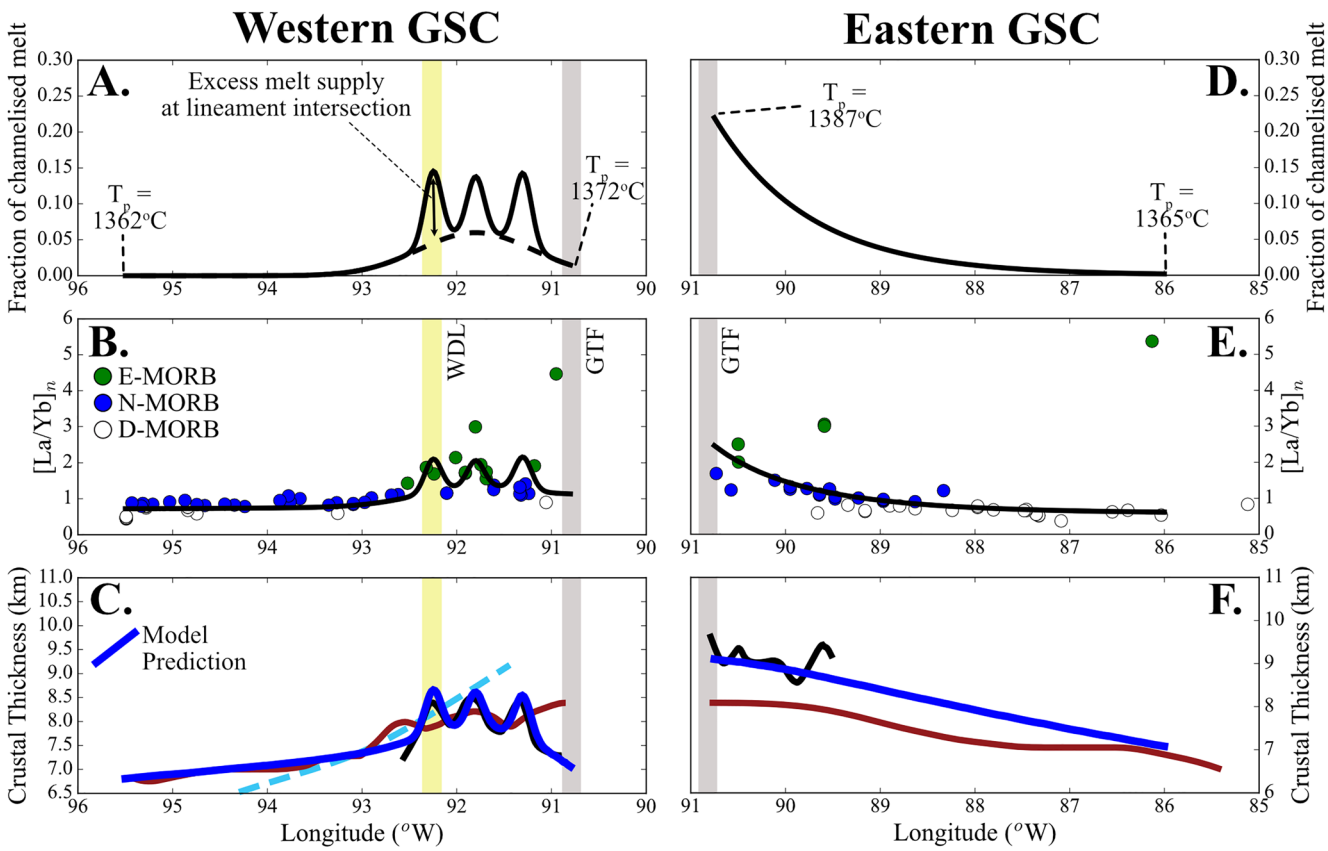

Figure 5. Results of plume-ridge interaction models that account for channelized melt transport between the Galápagos mantle plume and the GSC. Panels (a)–(c) show the results for the western GSC and panels (d)–(f) show the results for the eastern GSC. Panels (a) and (d) show the input parameters for these models (i.e., the fraction of channelized melt), and the geochemical (b and e) and crustal thickness (c and f) results are shown below. Crustal thickness estimates are from Ito and Lin (1995; red), Canales et al. (2002; blue dashed), and Mittelstaedt et al. (2014; black); modeled crustal thickness is shown in blue (solid line). It can be observed that, by assuming channelized flow occurs beneath the volcanic lineaments of the Northern Galápagos Volcanic Province, the crustal thickness and geochemical signature of the basalts from the western GSC are more accurately reproduced in this model than in the model of solid-state plume-ridge interaction shown in Figure 4.

new mantle melting models which incorporate experimental constraints on F partitioning during mantle melting (Dalou et al., 2012) reveal that a pyroxenitic source F concentration >80 ppm overestimates the F/Nd ratio of the most enriched GSC basalts (owing to the slightly less compatible nature of F relative to Nd during melting of a pyroxenitic lithology; Figure 2d; Supporting Information S1). To provide more robust constraints on the F content of the pyroxenitic mantle source, we iteratively adjusted the concentration of F in our mantle melting models until the model predictions (generated by varying the proportion of plume-derived channelized melt to the GSC; see Section 6) matched the GSC data. The results indicate that our new data is best matched when the pyroxenitic F content is set at ~70 ppm.

6. Numerical Models of Galápagos Plume-Ridge Interaction

6.1. Simulating Mantle Melting

Early models of plume-ridge interaction related compositional variations in plume-influenced MORBs to chemical heterogeneity on the scale of 10's–100's of km in the sub-ridge mantle (i.e., erupted magma compositions are directly related to the bulk composition of the underlying mantle; Schilling, 1991; Schilling et al., 1982, 2003; Verma & Schilling, 1982). Such models suggested that isotopically and incompatible trace element enriched plume material flows toward, and then along, the ridge axis where it becomes progressively diluted by mixing with ambient asthenosphere.

These early models recreated some of the geochemical features that are observed along plume-influenced ridges; however, dynamical models of plume-ridge interaction predict no significant solid-state mixing between plume and ambient mantle (Farnetani & Richards, 1995; Ito et al., 1997, 2003). For this reason, more recent studies of plume-ridge interaction have focused on a second class of model, where mantle heterogeneity is important on length-scales of ~1 km or less (Ingle et al., 2010; Ito & Mahoney, 2005). In this type of model, the solid sub-ridge mantle is composed of a near constant mixture of enriched, hydrous peridotite or pyroxenite "blebs" in a depleted (anhydrous) peridotite matrix. Owing to their different volatile contents and/or lithological properties, the enriched blebs undergo melting at greater depths than the surrounding anhydrous peridotite (Ingle et al., 2010; Ito & Mahoney, 2005). Previous studies which have applied these models to the GSC have concluded that variations in basalt chemistry and crustal thickness are due to intermediate scale variations in mantle flow and/or melt extraction from the underlying mantle (Ingle et al., 2010; Ito & Bianco, 2014; Ito & Mahoney, 2005; Shorttle et al., 2010).

To test the plausibility of a mixed lithology mantle in Galápagos plume-ridge interaction, we use the pymelt module of Matthews et al. (2020), which simulates melting of peridotite and silica-deficient pyroxenite (KG1). We build on this model by calculating the trace element composition of basaltic melts formed beneath the ridge axis (see Supporting Information S1) and include calculations that account for the contribution of channelized melts formed by melting of a pyroxene-rich mantle component in the Galápagos plume stem. By simulating the melting of a mixed lithology mantle, our models differ from those of previous studies that have considered only volatile-bearing peridotite source components (Gibson & Richards, 2018; Ingle et al., 2010).

Our new models allow us to test the influence of plume-driven active upwelling; the depth at which melting ceases; and the contribution of channelized, plume-derived melts on the crustal thickness of the ridge and the trace element chemistry of the GSC basalts (see Supporting Information S1 for full model details). To do so, we calculate the hypothetical composition of magmas produced at ~0.05° intervals along the GSC, with variations in key mantle parameters (such as T_P; U_r–the relative horizontal velocity of mantle material exiting the melting region (Ingle et al., 2010; Ito & Mahoney, 2005); and the contribution of channelized plume-derived melts) tested to determine the dominant mechanism of plume-ridge interaction in the Galápagos. Notably, the value of U_r in all models shown here is depth dependent, following the relationship between U_r and pressure outlined by Ingle et al. (2010). Specifically, at pressures less than that of the anhydrous peridotite solidus U_r is set to 1, but at greater pressures this value is defined by the equation (derived from the work of Ito & Mahoney, 2005):

$$U_r(z) = 1 + 2 \times \left(\frac{z}{H}\right) - \left(\frac{z}{H}\right)^2$$

where z represents the depth below the anhydrous perioditite solidus and H is the depth interval that separates the initiation of mantle melting from the anhydrous peridotite solidus (see Supporting Information S1). $U_{r\text{-max}}$ is used in this study to define the maximum value of U_r beneath each area of the GSC (i.e., at the base of the melting region).

Here, we examine the extent to which the long and short length-scale geochemical and geophysical features of plume-ridge interaction on the GSC can be recreated if we assume only solid-state flow between the Galápagos mantle plume and GSC, as proposed by Ingle et al. (2010), Shorttle et al. (2010), and Ito and Bianco (2014). We then highlight areas where solid-state plume-ridge interaction models poorly match the available data, and examine whether additional transport of volatile-rich melts in long-lived melt channels (Gibson & Richards, 2018) can account for these discrepancies.

The initial non-volatile trace element composition of the various mantle components beneath the GSC are set as the depleted DMM (Workman & Hart, 2005), a 90:10 mixture between the depleted DMM and an enriched mantle component (Donnelly et al., 2004), and an estimate for the trace element composition of a silica-deficient pyroxenite (based on the composition of the KG1 pyroxenite presented by Lambart, 2017) for the eastern GSC peridotite component, the western GSC peridotite component, and the enriched pyroxenitic component, respectively. In all of our models, the trace element partition coefficients were taken

from Gibson and Geist (2010) and mineral-melt partition coefficients for H_2O and F were taken from recent experimental data (Dalou et al., 2012; Rosenthal et al., 2015).

We recognize that melting parameterizations for silica-deficient pyroxenite in pymelt (Matthews et al., 2020) do not consider the effects of volatiles on the pyroxenite solidus. Analyses of natural samples of mantle pyroxenites have, however, shown that they have a greater capacity to host volatiles than peridotites (Gibson et al., 2020). The influence of elevated H_2O contents on the pyroxenitic solidus remains uncertain, although some experimental data indicate that the depression in the solidus temperature caused by the presence of H_2O in a pyroxenitic mantle source is less than that seen in peridotitic source components (Sorbadere et al., 2013). Nevertheless, more experimental work is required to accurately parameterize the effects of H_2O on pyroxenite melting, as has been done for peridotites (Katz et al., 2003). In our forward models of fractional melting, we have used a H_2O estimate of 550 ppm for the pyroxenite source, as this reproduces the volatile versus trace element systematics of the GSC basalts (see Section 5). We accept, however, that because of uncertainties in the depth of melting of volatile-bearing pyroxenite this is a non-unique solution.

6.2. Along-Ridge Variations in GSC Basalt Geochemistry and Crustal Thickness Predicted by Solid-State Flow

In the models of solid-state plume-ridge interaction shown below, it is assumed that variations in basalt chemistry and crustal thickness along the GSC are related to changes in the rate of mantle flow below the anhydrous peridotite solidus and/or variations in source ratios (Cushman et al., 2004; Gibson & Richards, 2018; Ingle et al., 2010; Ito & Bianco, 2014; Maclennan et al., 2001; Shorttle et al., 2010). Variations in mantle upwelling velocity below the anhydrous peridotite solidus are hypothesized to occur as a result of the excess buoyancy flux of mantle plumes and the rapid increase in mantle viscosity associated with olivine dehydration following the onset of mantle melting (Hirth & Kohlstedt, 1996, 2003). In addition, although dynamical models of plume-ridge interaction indicate that that there will be limited mixing between plume material and the surrounding ambient mantle in the asthenosphere (Ito et al., 1997), variations in source proportions beneath the GSC are considered owing to the clear spatial heterogeneity in the composition of the Galápagos mantle plume (Gleeson et al., 2021; Harpp & Weis, 2020; Harpp & White, 2001; White et al., 1993).

In the following solid-state plume-ridge interaction models, the relative rate at which mantle material exits the melting region at the base of the melt column ($U_{r\text{-max}}$; horizontal velocity relative to a scenario where no active upwelling is present) is assumed to decrease with increasing distance from the GTF (Table 1). This relationship (between $U_{r\text{-max}}$ and longitude) is selected following the study of Ingle et al. (2010) and qualitatively follows the change in mantle flow velocities predicted by the numerical models of Bianco et al. (2013) and Ito and Bianco (2014). Similarly, we test various relationships between longitude and the mantle potential temperature (T_p), the mass fraction of pyroxenitic material in the source, and the pressure at the base of the lithosphere/top of the melt column.

We iteratively adjusted these parameters until our models produced a satisfactory match to both the composition of the GSC basalts and the crustal thickness estimates of Canales et al. (2002) and Mittelstaedt et al. (2014). Example model results are shown in Figure 4 and Table 1 and indicate that solid-state plume-ridge interaction produces an excellent match to the composition of most basalts erupted west of 86°W on the eastern GSC, and the D-MORBs and N-MORBs located on the western GSC. In addition, the model results reveal clear differences between the eastern and western GSC. For example, to generate the greater crustal thickness of the oceanic crust produced along the eastern GSC (Mittelstaedt et al., 2014), our models indicate that the mantle potential temperature beneath the eastern GSC adjacent to the GTF is slightly higher (~5°C) than at any point beneath the western GSC. The change in crustal thickness along each ridge segment (i.e., the eastern and western GSC) is driven by a combination of changes in mantle potential temperature (~10°C), the proportion of pyroxenite in the mantle source and contribution of plume-driven upwelling in regions closest to the GTF. Additionally, our results indicate that the pressure at the top of the melting region is greater in regions adjacent to the GTF, possibly owing to conductive cooling effects of the cold lithospheric material of the transform fault (Le Voyer et al., 2015) and the increased proportion of pyroxenite in the mantle source (Brunelli et al., 2018). This increase in the pressure of melt termination is

Table 1
Parameters Used in the Solid-State and Melt Channelization Models of Plume-Ridge Interaction (Shown in Figures 4 and 5, Respectively)

	Solid-state models		Melt channelization models	
Parameter	Western GSC	Eastern GSC	Western GSC	Eastern GSC
T_p at GTF (°C)	1370	1375	1372	1387
T_p distal from GTF (°C)	1360	1365	1362	1365
$U_{r\text{-max}}$ at GTF	7	8	2.5	1.8
A[a]	0.6	0.5	0.6	0.4
B[a]	6	8	1.5	0.8
C[a]	0	0	0	0
X_{Pyx} at GTF	0.10	0.10	0.06	0.08
A	0.4	0.4	0.4	0.3
B	0.08	0.09	0.04	0.06
C	0.02	0.01	0.02	0.02
$P_{termination}$ (GPa)[b] at GTF	0.65	0.7	0.43	0.6
A	1.5	1.5	1.5	1.2
B	0.40	0.45	0.18	0.35
C	0.25	0.25	0.25	0.25
H_2O (peridotite)	145	100	145	100
H_2O (pyroxenite)	550	550	550	550
T_p for generation of channelized melts	n/a	n/a	1400	1400

[a]$U_{r\text{-max}}$, X_{Pyx}, and $P_{termination}$ are calculated according to $\left(U_{r\text{-max}}, X_{Pyx}, P_{termination}\right) = \exp\left(-\left(\left(\text{Long}\left(°\text{W}\right) - 90.8\right) \times A\right)\right) \times B + C$ on the western GSC and $\left(U_{r\text{-max}}, X_{Pyx}, P_{termination}\right) = \exp\left(-\left(\left(90.8 - \text{Long}\left(°\text{W}\right)\right) \times A\right)\right) \times B + C$ on the eastern GSC. [b]$P_{termination}$ (GPa) refers to the pressure at the top of the melt column.

required to avoid a "run-away" increase in the crustal thickness of the ridge in regions where the contribution of active plume driven upwelling is greatest.

Figure 4 also highlights several pitfalls that are associated with solid-state plume-ridge interaction models that account for lateral variations in mantle flow. For example, modeled crustal thickness increases systematically along the western GSC toward the GTF, which is qualitatively consistent with the crustal thickness variations predicted in numerical simulations of mantle flow for on-axis (or near-axis) mantle plumes (e.g., Iceland; Bianco et al., 2013). Recent studies have, however, shown that there are three ~20 km wide regions between ~92.5°W and the GTF with crustal thickness anomalies of ~1 km (Mittelstaedt et al., 2014), which our simple model of solid-state plume-ridge interaction cannot capture (Figure 4). In addition, although the solid-state plume-ridge interaction model shown in Figure 4 accurately recreates the chemistry of the western GSC N-MORBs located west of 92.5°W and east of 91.8°W, they are not able to recreate the composition of the more enriched basalts located between 92.5° and 91.8°W, or the composition of anomalously enriched basalts that are present between 89.5° and 92°W on the GSC.

Some of these discrepancies may be addressed if we consider non-symmetric spreading of solid plume material. One possible mechanism that might facilitate such flow is thermal erosion of a sub-lithospheric channel between the mantle plume and adjacent ridge (Kingsley & Schilling, 1998; Schilling, 1991). However, geophysical and petrological estimates indicate that there are no areas of significant (i.e., >10 km) lithospheric thinning beneath the volcanic lineaments connecting the western GSC to the Galápagos Archipelago (Gibson & Geist, 2010; Harpp, Wirth, et al., 2014). Therefore, any thermal erosion of the lithosphere beneath the northern Galapagos is unlikely to be sufficient to trap plume material and influence plume outflow (cf. Gibson et al., 2015). In addition, some of the offsets between our model predictions and the GSC data may result from the use of a 2D model scenario to describe a 3D system. In particular, the influence of transform faults on upper mantle dynamics is not considered here, but could influence the composition of

basalts erupted close to these structures (Weatherley & Katz, 2010), and the eastward motion of the Nazca plate above the Galápagos plume stem is likely to cause some deflection of solid plume material in the upper mantle (e.g., Harpp & White, 2001). Nevertheless, we believe that these factors are unlikely to account for the shortcomings of the solid-state plume ridge interaction models.

6.3. Channelized Flow of H_2O-Rich Melts to the GSC

Numerical models of mantle melting beneath oceanic spreading centers have shown that highly permeable melt channels are a natural consequence of melting during upwelling of a heterogeneous mantle (Katz & Weatherley, 2012; Weatherley & Katz, 2012). As chemical interaction of channelized melts with the surrounding mantle is expected to be limited (Weatherley & Katz, 2012), channelized melt flow might represent an efficient method of transporting geochemically enriched material to nearby spreading centers. In addition, highly permeable melt channels have been shown to be thermodynamically stable over distances up to ~1,500 km (for channels ~50–60m in radius) and the transport timescales of volatile-rich melts in these channels are significantly lower than the timescales required by U-series disequilibria (Kokfelt et al., 2005; Mittal & Richards, 2017). Therefore, conceptual models involving the delivery of plume-derived compositionally enriched melts to MORs in highly permeable melt channels have been proposed for the Galápagos and other sites of plume-ridge interaction worldwide (e.g., associated with the Azores, Discovery, Easter, and Reunion mantle plumes; Gibson et al., 2015; Gibson & Richards, 2018; Mittal & Richards, 2017). In these models, the primary factor driving the migration of melts from the stem of the upwelling plume (>60–80 km depth) to the sub-ridge mantle (<40–60 km depth) is melt buoyancy. Melt channelization was likely initiated when the Galápagos plume was on-axis (at >5 Ma) and has been maintained during ridge migration away from the plume stem (Gibson et al., 2015).

6.3.1. Variations in the Supply of Channelized Melts to the Western and Eastern GSC

The solid-state plume-ridge interaction models described in Section 6.2 require relative horizontal flow velocities at the base of the melting region ($U_{r\text{-max}}$) of ~6–8 to explain the geochemical and geophysical signatures of plume-ridge interaction between 90.5° and 90.8°W (Figure 4). Values of $U_{r\text{-max}}$ up to ~15 have previously been suggested for the GSC, based on the buoyancy flux of the Galápagos mantle plume (Ingle et al., 2010; Sleep, 1990).

In the following models, however, we assume that: (a) the change in the relative mantle flow velocity below the anhydrous peridotite solidus is small ($U_{r\text{-max}} < 1.5$–2.5) and (b) variations in the geochemical and geophysical signatures of plume-ridge interaction along the GSC are instead derived from slight changes in T_P and/or the supply of channelized melts from the Galápagos plume stem (Table 1). The volatile and non-volatile trace element composition of the channelized melts are calculated as the non-modal aggregated fractional melt of the enriched (pyroxenitic) mantle component (see Supporting Information S1 for detailed methods). We assume that the melt channels form at depths below the anhydrous peridotite solidus (>2.5–3 GPa at $T_P = 1400$°C) and various values for the pressure of channel initiation/formation were tested.

The crustal thickness and geochemical characteristics of the eastern GSC are generally well-matched by our solid-state models of plume-ridge interaction. Nevertheless, we recognize that this is not a unique solution as these observations can also be reproduced if we model an exponential decrease in the proportion of channelized melts supplied to the eastern GSC with increasing distance to the center of plume upwelling (Figure 5). In this model, the decrease in the supply of channelized, enriched melt to the eastern GSC with increasing distance to the Galapagos plume may be related to a decline in the number of melt channels that remain thermodynamically stable over the increased plume-ride distance (Mittal & Richards, 2017), or changes in the angle at which melt channels intersect the ridge axis (i.e., assuming the melt channels initiate from a single location beneath the Galápagos Archipelago, the melt channels may be orientated roughly perpendicular to the ridge axis near the GTF but this orientation is not maintained further east; Figure 6). This hypothesis shares many similarities to the model proposed for solid-state plume-ridge interaction by Shorttle et al. (2010) but has the advantage of being able to simultaneously explain the enriched geochemical signatures along the GSC and the depleted isotopic compositions of the island of Marchena and Genovesa in the Northern Galápagos Volcanic Province (Gibson et al., 2015; Harpp, Wirth, et al., 2014).

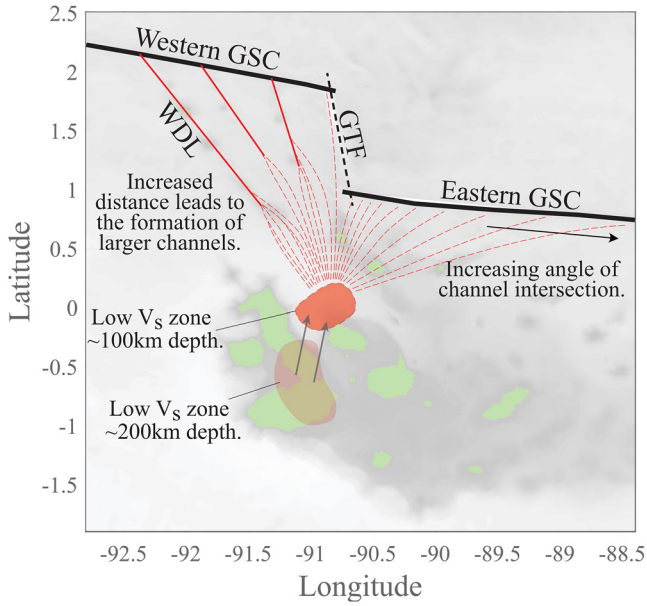

Figure 6. Schematic diagram illustrating the nature of the melt channels beneath the northern Galápagos volcanic province. The eastern GSC is fed by a large number of small melt channels and the influence of these melt channels declines with increasing distance to the mantle plume. On the western GSC our models predict that the melt channels amalgamate into three larger channels that are located beneath each of the three volcanic lineaments in the northern Galápagos volcanic province. The location of the Galápagos mantle plume at depths of 200 and 100 km is taken from Villagómez et al. (2014).

At the closest point to the Galápagos Archipelago, the eastern GSC is located only ~100–150 km north of the center of plume upwelling, identified at 100 km depth in the seismic tomography study of Villagómez et al. (2014). In their theoretical study, Mittal and Richards (2017) showed that over such short plume-ridge separation distances, melt channels ~5 m in radius are likely to be thermodynamically stable (assuming a constant heat flux source). This radius is within the range observed in dunitic/melt channels observed in ophiolites worldwide (e.g., dunitic channels in the Oman ophiolite can reach 200 m across; Kelemen et al., 1997). We suggest, therefore, that the delivery of compositionally enriched melts to the eastern GSC in highly permeable melt channels only a few meters in thickness could generate the geochemical enrichment observed along the eastern GSC. The continued presence of channelized melts along the whole of the eastern GSC, even if only in very small proportions (<1%), maintains the possibility that anomalously enriched basalts can be observed at the surface at plume-ridge interaction distances in excess of 300–400 km (see Section 6.3.2). However, while the geochemical and geophysical features observed on the eastern GSC can be produced by both solid-state and melt transport models of plume ridge interaction, many of the discrepancies between the GSC data and solid-state models of plume-ridge interaction occur on the western GSC (e.g., the composition of basalts located between 92.5° and 91.8°W).

Our models reveal that the geochemical and geophysical signatures of plume-ridge interaction on the western GSC cannot be produced by a similar model to that used to recreate the eastern GSC data (i.e., a gradually decreasing supply of channelized melts with increasing plume-ridge distance). Instead, we find that the discrepancies between the western GSC geochemical and geophysical data and our solid-state plume-ridge interaction models can be overcome by simulating a low level of channelized melt contribution to the western GSC between ~93°W and the GTF (<10% channelized melt contribution) and focused delivery of additional channelized melts to the western GSC beneath each of the three volcanic lineaments in the northern Galápagos (Figure 5), as proposed by Mittal and Richards (2017) and Gibson and Richards (2018). In the model used here, the proportion of channelized melt supplied to the western GSC beneath each of the lineaments is assumed to follow 3 overlapping normal distributions, where the greatest rate of supply occurs at the intersection of each of the three volcanic lineaments with the GSC (92.25°W, 91.8°W, 91.3°W). The results provide an excellent match to the geochemical data (including volatiles) from the western GSC and reproduce the short length-scale variations in crustal thickness observed at the intersection of each volcanic lineament with the western GSC (Figure 5; Mittelstaedt et al., 2014). It is important to note, however, that the compositional variability between the different seamounts and islands that make up the three volcanic lineaments indicates that their magmatic systems are locally complex (Harpp, Wirth, et al., 2014).

Notably, the models used to recreate the geochemical and geophysical signatures of plume-ridge interaction along the western and eastern sections of the GSC are very different, although similar levels of geochemical enrichment are observed on both ridge segments. We propose that the differences may arise from the greater plume-ridge distance of the western GSC compared to the eastern GSC (~100 km greater). Specifically, we suggest that the large plume-ridge interaction distance of the western GSC results in the amalgamation of several melt channels into a focused region beneath each volcanic lineament (and thus localized delivery of channelized melt to the ridge axis). This coalescence may help to maintain the thermodynamic stability of the melt channels over the greater plume-ridge distance (Figure 6; Mittal & Richards, 2017), and is consistent with the amalgamation of high porosity (channelized) regions observed in numerical models of mantle melting (e.g., Katz & Weatherley, 2012). Nevertheless, the coincidence of a ~10 km wide crustal thickness anomaly (Mittelstaedt et al., 2014) and two anomalously volatile-rich samples (TR164 6D-1g and 2g, which lie outside the compositions predicted by our along-ridge models; Figure 5) on the eastern GSC at 89.59°W

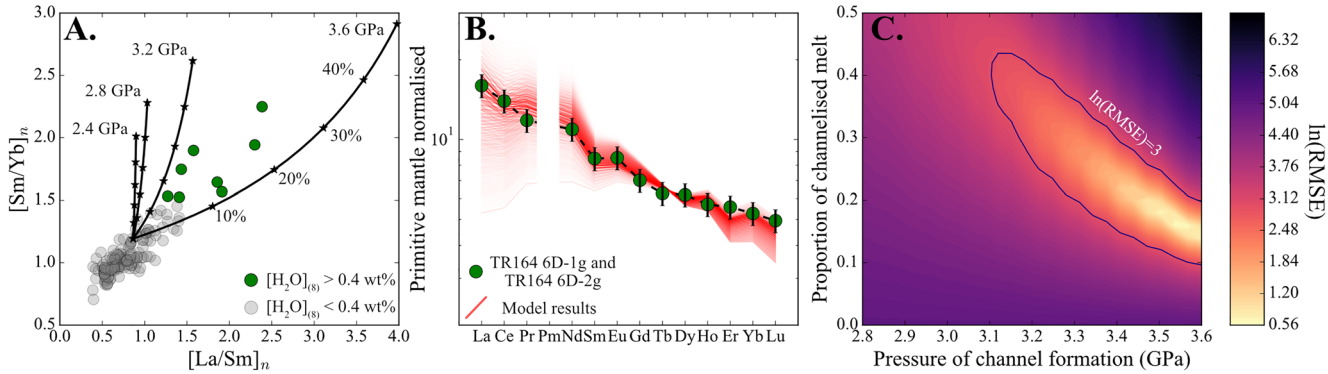

Figure 7. Comparison of our mantle melting models that include a contribution of plume-derived channelized melts to the composition of the anomalously enriched basalts from the GSC. (a) Composition of basalts that cannot be reproduced by our along-ridge models of plume-ridge interaction are shown in green and are generally characterized by $[H_2O]_{(8)}$ contents above 0.4 wt.%. The composition of these enriched basalts is best reproduced when the proportion of channelized melt is >15% and the depth of channel formation is >3.2 GPa. Notably, as the pymelt simulations do not account for the presence of H_2O on the pyroxenite solidus, parameterization of hydrous melting might influence our estimates for the pressure of channel formation. (b) Comparison of 676 models to the composition of the TR164 6D-1g and TR164 6D-2g basalts (89.59°W). The models with the lowest RMSE are shown by the darker colors. (c) RMSE for all models shown in (b) where the contribution of channelized melt is between 0% and 50%, and the pressure of channel formation is between 2.8 and 3.6 GPa. In all models, the composition of the channelized melts are calculated using a T_P of 1400°C and a pyroxenite source fraction of 20% (Gleeson et al., 2021).

indicate that localized variations in the volume of melt delivered to the eastern GSC exist. In addition, the sample density along the eastern GSC is lower than that along the western GSC, which raises the possibility that other short length-scale geochemical heterogeneities may be present in the region between 89.59 and 90.8°W, but are unsampled. As such, more data is required to confirm that differences in the characteristics of melt channelization to the western and eastern GSC control the geochemical and geophysical features of plume-ridge interaction in the Galápagos.

6.3.2. Anomalously Enriched GSC Basalts

The above models of plume-ridge interaction via channelized transport of volatile-rich melts accurately recreate the broad-scale, and some of the short length-scale, geochemical and geophysical features of plume influence on the GSC. There are, however, a series of basalts located along plume-influenced segments of the GSC (and in other regions of plume-ridge interaction worldwide) that display compositions which are too enriched to be explained by any of the models outlined above (e.g., TR164 6d-1g at 89.59°W; Gibson & Richards, 2018). These anomalously enriched basalts, which typically contain $[H_2O]_{(8)}$ contents >0.4 wt.%, have previously been explained through the localized delivery of large volumes of channelized melt to the ridge, overwhelming the contribution of more depleted melts formed in the shallow mantle (Gibson & Richards, 2018; Mittal & Richards, 2017). To build on this previous work, we compared the results of our mantle melting models that incorporate the presence of channelized, plume-derived melts to the composition of the anomalously enriched basalts located along the GSC.

In detail, we calculated the Root Mean Squared Error (RMSE) between our mantle melting models and each of the anomalously enriched GSC basalts. The mantle potential temperature of the Galápagos plume (where the channelized melts are being formed) is set at 1400°C in all calculations, and we tested variations in the contribution of channelized melt (0%–50%), and the pressure of channel formation (2.8–3.6 GPa). This pressure range was chosen as initial models showing the influence of incorporating plume-derived channelized melts demonstrated that channel formation at lower pressures is unable to recreate the high $[La/Sm]_n$ ratio of the anomalously enriched GSC basalts (Figure 7a). The proportion of pyroxenite in the Galapagos plume stem was set at ~20% (Gleeson et al., 2021).

The model calculations demonstrate that the anomalously enriched basalts from the GSC, which have $[H_2O]_{(8)}$ contents >0.4 wt.%, likely contain a >15% contribution of channelized, plume-derived melts (Figure 7). However, the large proportion of channelized melt required to recreate the composition of these anomalously enriched basalts is inconsistent with the magnitude of the crustal thickness anomalies found in these locations (Mittelstaedt et al., 2014). For example, at ~89.59°W on the eastern GSC, where a crustal thickness anomaly of ~0.5–1 km is observed (~9.5 km thick crust compared to the model predictions of ~8.5–9 km),

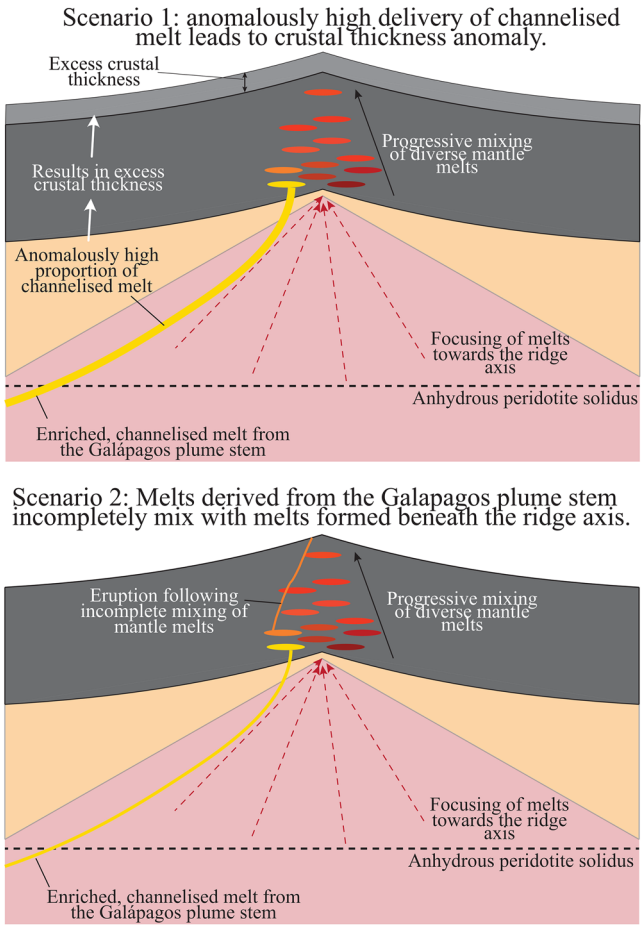

Figure 8. Schematic diagram displaying the two ways in which delivery of channelized melt might contribute to the geochemical and geophysical parameters (such as crustal thickness) observed along the GSC. In scenario 1, an anomalously high flux of channelized melt to the GSC results in moderately-to-highly enriched basalts at the surface and anomalously thick crust (e.g., at the intersection of the WDL with the GSC). In scenario 2, only a moderate supply of channelized melt exists. However, some of this channelized melt manages to ascend and erupt without completely mixing and/or homogenizing with melts formed beneath the ridge axis leading to the presence of anomalously enriched basalts at the surface.

the >15% contribution of channelized melt required to reproduce the geochemical signature of the highly enriched GSC basalts would, in theory, generate a crustal thickness anomaly >1–1.5 km (Figure 7). The discrepancy between the predicted and observed crustal thickness is even greater at the location of sample TR164 26D-3g (90.95°W) where no crustal thickness anomaly is observed, but a >30% contribution of channelized melt is required to reproduce the trace and volatile element systematics of the erupted basalt.

We therefore suggest that the high proportion of channelized melt that contributes to the composition of the most volatile-rich GSC basalts is a result of inefficient mixing of channelized melts with more depleted magmas produced at shallower depths in the sub-ridge mantle (Figure 8). This scenario that is consistent with the proposed chemical isolation of high-pressure channelized melts with the surrounding mantle peridotite during magma transport (Katz & Weatherley, 2012; Keller & Katz, 2016). In this scenario, volatile-rich basaltic magmas may reach the surface even in regions where there is a relatively low flux of channelized plume-derived melts to the GSC (Figure 8). In fact, the low melt flux at large plume-ridge interaction distances (e.g., sample ST7 17D-1g; 86.13°W), and locations that are proximal to large transform faults (e.g., samples TR164 26D-3g; 90.95°W, respectively), might restrict the formation of a steady-state magma chambers (Le Voyer et al., 2015; Sinton & Detrick, 1992). As a result, it is possible that magma homogenization is subdued at these locations, increasing the probability of enriched basalts being observed at the surface (Langmuir & Bender, 1984; Le Voyer et al., 2015).

7. Quantifying the Outflux of H_2O on Plume-Influenced Sections of the Galápagos Spreading Center

Our new volatile data expand the small number of analyses previously published for the eastern GSC (e.g., Byers et al., 1983), and extend the existing GSC database of volatile element analyses to cover the entire region of plume-influenced ridge. Nevertheless, for many basalts erupted along plume-influenced sections of the GSC, volatile data are absent and we thus use the available fractional crystallization-corrected H_2O data from both the eastern and western GSC to identify a non-volatile trace element proxy that can be used to estimate the H_2O contents of the remaining GSC basalts.

The $[H_2O]_{(8)}$ (that is, the water concentration of each sample once it has been fractional crystallization corrected to 8 wt.% MgO) and $[Sm/Yb]_n$ contents of basalts from both the western and eastern GSC display a positive correlation ($r^2 = 0.907$; Figure 3a). As such, we use the $[Sm/Yb]_n$ ratio of the GSC basalts as a proxy for their fractionation corrected H_2O contents ($[H_2O]_{(8)}$). $[Sm/Yb]_n$ is chosen rather than $[Ce/Yb]_n$, as suggested by Gibson and Richards (2018), because our new data shows a small number of highly enriched basalts from the western GSC have slightly higher $[H_2O]_{(8)}$ at a given $[Ce/Yb]_n$ than the other GSC basalts (Figure 3b). As a result, the correlation between $[H_2O]_{(8)}$ and $[Ce/Yb]_n$ is subtly different for basalts from the eastern and western GSC (gradients of 0.142 and 0.162, respectively; Figure 3b).

Taking our new volatile data from the eastern GSC, together with published volatile data from the western GSC (Cushman et al., 2004; Ingle et al., 2010), and estimated volatile contents based on the trace element content of additional GSC basalts (Christie et al., 2005), we can use our two component models of plume-ridge interaction to calculate the outflux of H_2O from plume-influenced sections of the GSC. This is achieved using our along-ridge mantle melting models that incorporate the influence of channelized melt

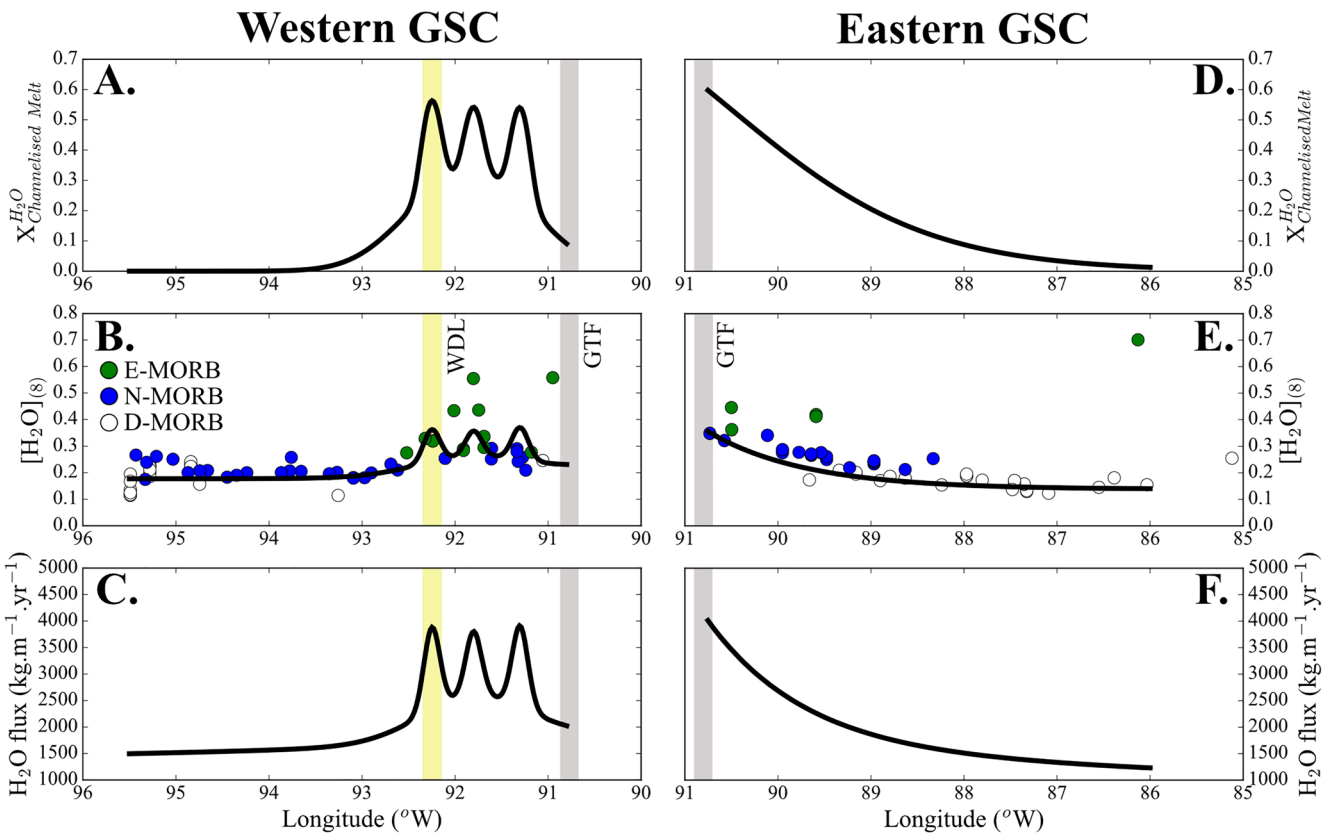

Figure 9. H_2O concentrations and fluxes predicted by new models of plume-ridge interaction in the Galápagos (models are identical to those shown in Figure 5). The model accurately recreates the H_2O contents of basalts from both the eastern GSC and the western GSC (model results assume ~20% fractionation of olivine and/or plagioclase). The maximum outflux of H_2O along the western GSC is ~4,000 kg/m/year where the volcanic lineaments intersect the GSC (compared to the background flux of only ~2,000 kg/m/year). The greatest outflux of H_2O from the GSC is observed on the eastern GSC near the GTF (~4,000 kg/m/year) and, in this location, ~60% of the H_2O flux out of the GSC is sourced from plume-derived channelized melts.

transport and accurately recreate the trace element composition and crustal thickness of the plume-influenced GSC, alongside the following equation:

$$H_2O^{flux}\left(kg\ /\left(m\ year\right)\right) = \left(C_{H_2O}^{mix}\left(ppm\right)\times 10^{-6}\right)\times SR\left(m\ /\ year\right)\times CT\left(m\right)\times 2900\left(kg\ /\ m^3\right)$$

where $C_{H_2O}^{mix}$ is the H_2O concentration of the fully homogenized primary mantle melts and CT is the crustal thickness produced at each calculation interval along the GSC (calculation step size of ~0.05°). SR represents the spreading rate of the GSC (Schilling et al., 2003), and the density of the melt phase is assumed to be ~2,900 kg/m^3.

Our results indicate that incorporation of enriched material from the Galápagos mantle plume causes the flux of H_2O to increase by a factor of 3 from 86 to 90.8°W on the eastern GSC (Figure 9). On the western GSC, the flux of H_2O is greatest in regions where the volcanic lineaments intersect the GSC, and the maximum flux of H_2O from any part of the western GSC is similar to the maximum H_2O flux along the eastern GSC (~4,000 kg/m/year; Figure 9). In addition, our calculations show that volatile-rich channelized melts contribute up to ~60% of the H_2O and F outflux, from localized regions of the plume-influenced GSC (Figure 9; Supporting Information S1). Overall, melt channelization may account for ~35% of the H_2O outflux from the western GSC between 90.8 and 92.5°W and ~25% of the H_2O outflux between 86° and 90.8°W on the eastern GSC.

While transport of volatile-rich melts to the GSC has a clear influence on the H_2O and F concentrations of the erupted magmas, little to no variations are seen in the $^3He/^4He$ ratio of these basalts (Graham et al., 2014). This observation requires that melts reaching the GSC have much lower $^3He/^4He$ than those forming deep

in the plume beneath the western Galápagos Archipelago. The lack of a primordial $^3He/^4He$ signature in plume-influenced GSC basalts may be because: (a) rapid vertical transport of high-pressure melts with elevated $^3He/^4He$ ratios is restricted to the vicinity of the plume stem (Kurz & Geist, 1999; Peterson et al., 2017; Villagómez et al., 2014) or (b) the "deep" plume-stem melts that are being transported laterally to the ridge via channelized flow may be derived from blebs of recycled lithosphere (Gleeson et al., 2020) with similar or lower $^3He/^4He$ ratios to MORBs (e.g., Day et al., 2015).

8. Conclusions

Our study uses new analyses of volatiles (H_2O, F, Cl, and S) in basaltic glass chips from the GSC, as well as two-component mantle melting models, to investigate the nature and dynamics of plume-ridge interaction in the Galápagos. The results of this study can be summarized in 4 key points:

1. Solid-state transfer of plume material between the Galápagos mantle plume and adjacent GSC can account for some of the long length-scale (~100–1,000 km wide) geochemical and geophysical signatures of plume-ridge interaction. However, solid-state plume-ridge interaction models cannot easily explain the presence of short length-scale (<10 km) geochemical and geophysical heterogeneities.
2. The long and short length-scale features of plume-ridge interaction in the Galápagos are readily explained by plume-ridge interaction models that include the transport of volatile-rich melts to the GSC in melt-dominated channels.
3. One key feature of plume-influenced ridge segments is the presence of anomalously enriched basalts, that is, those that are substantially more enriched with respect to their trace element contents than their neighboring basalts (e.g., Gibson & Richards, 2018). The strongly enriched basalts on the GSC also have anomalously high Fe isotope ratios that have been interpreted as reflecting large contributions of melt from a pyroxenitic mantle component within the Galápagos plume (Gleeson et al., 2020). While we acknowledge that the role of pyroxenite is controversial, and more work needs to be done, the key findings of our models for the mechanisms of plume-ridge interaction are, to a large extent, independent of the source lithology chosen for the enriched mantle component in the source region of the GSC basalts (i.e., peridotite vs. pyroxenite).
4. Our new mantle melting models indicate that the composition of the GSC basalts are controlled by the incomplete mixing of channelized, volatile-rich melts from the Galápagos mantle plume with more depleted melts formed by adiabatic decompression in the sub-ridge mantle. They also suggest that the most enriched basalts from the GSC may contain a >40% contribution from channelized, plume-derived melt.
5. Our results indicate that plume-ridge interaction causes the H_2O flux out of the GSC to vary by a factor of ~3, with the greatest amounts observed on the eastern GSC near the Galápagos Transform Fault and at the intersections of volcanic lineaments with the western GSC (up to ~4000 kg/m/year). We suggest that delivery of volatile-rich channelized melts to the ridge axis might account for up to ~60% of the H_2O flux out of these regions

Acknowledgments
M. L. M. Gleeson was supported by a NERC (Natural Environmental Research Council) Research Training Student Grant (NE/L002507/1) and a Research Fellowship funded by the Royal Commission for the Exhibition of 1851. S. A. Gibson was supported by grant RG57434 for research in Galápagos. We are grateful to Iris Buisman and Richard Hinton for assistance with EPMA and SIMS analysis, respectively. The Secondary Ion Mass Spectrometry analysis was carried out at the Edinburgh Ion Microprobe Facility (award IMF622/0517). The authors thank Mike Stock for his help with SIMS data collection and early discussions about the project, as well as the Marine Geological Samples Laboratory at the University of Rhode Island for supplying the GSC samples. The authors are also grateful to M. A. Richards and T. Mittal for sharing their thoughts on plume-ridge interaction, together with K. Harpp, P. Michael, and an anonymous reviewer whose constructive comments greatly improved the quality of our manuscript.

Data Availability Statement

Data collected in this study, and the code used to analyse the data, can be found through https://zenodo.org/badge/latestdoi/379869011.

References

Asimow, P. D., & Langmuir, C. H. (2003). The importance of water to oceanic mantle melting regimes. *Nature*, *421*, 815–820. https://doi.org/10.1038/nature01429

Behn, M. D., Sinton, J. M., & Detrick, R. S. (2004). Effect of the Galápagos hotspot on seafloor volcanism along the Galápagos Spreading Center (90.9–97.6°W). *Earth and Planetary Science Letters*, *217*, 331–347. https://doi.org/10.1016/S0012-821X(03)00611-3

Bianco, T. A., Ito, G., van Hunen, J., Mahoney, J. J., & Ballmer, M. D. (2013). Geochemical variations at ridge-centered hotspots caused by variable melting of a veined mantle plume. *Earth and Planetary Science Letters*, *371–372*, 191–202. https://doi.org/10.1016/j.epsl.2013.03.050

Blacic, T. M., Ito, G., Canales, J. P., Detrick, R. S., & Sinton, J. (2004). Constructing the crust along the Galapagos Spreading Center 91.3°–95.5°W: Correlation of seismic layer 2A with axial magma lens and topographic characteristics. *Journal of Geophysical Research*, *109*. https://doi.org/10.1029/2004JB003066

Braun, M. G., & Sohn, R. A. (2003). Melt migration in plume–ridge systems. *Earth and Planetary Science Letters*, *213*, 417–430. https://doi.org/10.1016/S0012-821X(03)00279-6

Brunelli, D., Cipriani, A., & Bonatti, E. (2018). Thermal effects of pyroxenites on mantle melting below mid-ocean ridges. *Nature Geoscience*, *11*, 7. https://doi.org/10.1038/s41561-018-0139-z

Byers, C. D., Muenow, D. W., & Garcia, M. O. (1983). Volatiles in basalts and andesites from the Galapagos Spreading Center, 85° to 86°W. *Geochimica et Cosmochimica Acta*, *47*, 1551–1558. https://doi.org/10.1016/0016-7037(83)90181-3

Cabral, R. A., Jackson, M. G., Koga, K. T., Rose-Koga, E. F., Hauri, E. H., Whitehouse, M. J., et al. (2014). Volatile cycling of H_2O, CO_2, F, and Cl in the HIMU mantle: A new window provided by melt inclusions from oceanic hot spot lavas at Mangaia, Cook Islands. *Geochemistry, Geophysics, Geosystems*, *15*, 4445–4467. https://doi.org/10.1002/2014GC005473

Canales, J. P., Dunn, R. A., Ito, G., Detrick, R. S., & Sallarès, V. (2014). Effect of variations in magma supply on the crustal structure of mid-ocean Ridges: Insights from the Western Galápagos Spreading Center. In K. S. Harpp, E. Mittelstaedt, N. d'Ozouville, & D. W. Graham (Eds.), *Geophysical monograph series* (pp. 363–391). John Wiley & Sons, Inc. https://doi.org/10.1002/9781118852538.ch17

Canales, J. P., Ito, G., Detrick, R. S., & Sinton, J. (2002). Crustal thickness along the western Galápagos Spreading Center and the compensation of the Galápagos hotspot swell. *Earth and Planetary Science Letters*, *203*, 311–327. https://doi.org/10.1016/S0012-821X(02)00843-9

Christie, D. M., Werner, R., Hauff, F., Hoernle, K., & Hanan, B. B. (2005). Morphological and geochemical variations along the eastern Galápagos Spreading Center. *Geochemistry, Geophysics, Geosystems*, *6*.

Cushman, B., Sinton, J., Ito, G., & Eaby Dixon, J. (2004). Glass compositions, plume-ridge interaction, and hydrous melting along the Galápagos Spreading Center, 90.5°W to 98°W. *Geochemistry, Geophysics, Geosystems*, *5*. https://doi.org/10.1029/2004GC000709

Dalou, C., Koga, K. T., Shimizu, N., Boulon, J., & Devidal, J.-L. (2012). Experimental determination of F and Cl partitioning between lherzolite and basaltic melt. *Contributions to Mineralogy and Petrology*, *163*, 591–609. https://doi.org/10.1007/s00410-011-0688-2

Danyushevsky, L. V., Eggins, S. M., Falloon, T. J., & Christie, D. M. (2000). H_2O abundance in depleted to moderately enriched mid-ocean ridge magmas; part I: Incompatible behaviour, implications for mantle storage, and origin of regional variations. *Journal of Petrology*, *41*, 1329–1364. https://doi.org/10.1093/petrology/41.8.1329

Day, J. M. D., Barry, P. H., Hilton, D. R., Burgess, R., Pearson, D. G., & Taylor, L. A. (2015). The helium flux from the continents and ubiquity of low-$^3He/^4He$ recycled crust and lithosphere. *Geochimica et Cosmochimica Acta*, *153*, 116–133. https://doi.org/10.1016/j.gca.2015.01.008

Detrick, R. S., Sinton, J. M., Ito, G., Canales, J. P., Behn, M., Blacic, T., et al. (2002). Correlated geophysical, geochemical, and volcanological manifestations of plume-ridge interaction along the Galápagos Spreading Center. *Geochemistry, Geophysics, Geosystems*, *3*, 1–14. https://doi.org/10.1029/2002GC000350

Dixon, J. E. (1997). Degassing of alkalic basalts. *American Mineralogist*, *82*, 368–378. https://doi.org/10.2138/am-1997-3-415

Dixon, J. E., Bindeman, I. N., Kingsley, R. H., Simons, K. K., Le Roux, P. J., Hajewski, T. R., et al. (2017). Light stable isotopic compositions of enriched mantle sources: Resolving the dehydration paradox. *Geochemistry, Geophysics, Geosystems*, *18*, 3801–3839. https://doi.org/10.1002/2016GC006743

Donnelly, K. E., Goldstein, S. L., Langmuir, C. H., & Spiegelman, M. (2004). Origin of enriched ocean ridge basalts and implications for mantle dynamics. *Earth and Planetary Science Letters*, *226*, 347–366. https://doi.org/10.1016/j.epsl.2004.07.019

Farnetani, D. G., & Richards, M. A. (1995). Thermal entrainment and melting in mantle plumes. *Earth and Planetary Science Letters*, *136*, 251–267. https://doi.org/10.1016/0012-821X(95)00158-9

Geist, D., Naumann, T., & Larson, P. (1998). Evolution of Galapagos magmas: Mantle and crustal fractionation without assimilation. *Journal of Petrology*, *39*, 953–971. https://doi.org/10.1093/petroj/39.5.953

Gibson, S. A., Dale, C. W., Geist, D. J., Day, J. A., Brügmann, G., & Harpp, K. S. (2016). The influence of melt flux and crustal processing on Re-Os isotope systematics of ocean island basalts: Constraints from Galápagos. *Earth and Planetary Science Letters*, *449*, 345–359. https://doi.org/10.1016/j.epsl.2016.05.021

Gibson, S. A., & Geist, D. (2010). Geochemical and geophysical estimates of lithospheric thickness variation beneath Galápagos. *Earth and Planetary Science Letters*, *300*, 275–286. https://doi.org/10.1016/j.epsl.2010.10.002

Gibson, S. A., Geist, D. J., & Richards, M. A. (2015). Mantle plume capture, anchoring, and outflow during Galápagos plume-ridge interaction: Mantle plume capture & outflow. *Geochemistry, Geophysics, Geosystems*, *16*, 1634–1655. https://doi.org/10.1002/2015GC005723

Gibson, S. A., & Richards, M. A. (2018). Delivery of deep-sourced, volatile-rich plume material to the global ridge system. *Earth and Planetary Science Letters*, *499*, 205–218. https://doi.org/10.1016/j.epsl.2018.07.028

Gibson, S. A., Rooks, E. E., Day, J. A., Petrone, C. M., & Leat, P. T. (2020). The role of sub-continental mantle as both "sink" and "source" in deep Earth volatile cycles. *Geochimica et Cosmochimica Acta*, *275*, 140–162. https://doi.org/10.1016/j.gca.2020.02.018

Gleeson, M., Soderman, C., Matthews, S., Cottaar, S., & Gibson, S. (2021). Geochemical constraints on the structure of the Earth's deep mantle and the origin of the LLSVPs. *Geochemistry, Geophysics, Geosystems*, *22*. https://doi.org/10.1029/2021GC009932

Gleeson, M. L. M., & Gibson, S. A. (2019). Crustal controls on apparent mantle pyroxenite signals in ocean-island basalts. *Geology*, *47*, 321–324. https://doi.org/10.1130/G45759.1

Gleeson, M. L. M., Gibson, S. A., & Williams, H. M. (2020). Novel insights from Fe-isotopes into the lithological heterogeneity of Ocean Island Basalts and plume-influenced MORBs. *Earth and Planetary Science Letters*, *535*, 116114. https://doi.org/10.1016/j.epsl.2020.116114

Graham, D. W., Hanan, B. B., Lupton, J. E., Hoernle, K., Werner, R., Christie, D. M., & Sinton, J. M. (2014). Helium isotope variations and mantle plume-spreading ridge interactions along the Galápagos Spreading Center. In K. S. Harpp, E. Mittelstaedt, N. d'Ozouville, & D. W. Graham (Eds.), *Geophysical Monograph series* (pp. 393–414). John Wiley & Sons, Inc. https://doi.org/10.1002/9781118852538.ch18

Hanan, B. B., & Graham, D. W. (1996). Lead and helium isotope evidence from oceanic basalts for a common deep source of mantle plumes. *Science*, *272*, 991–995. https://doi.org/10.1126/science.272.5264.991

Harpp, K. S., Geist, D. J., Koleszar, A. M., Christensen, B., Lyons, J., Sabga, M., & Rollins, N. (2014). The geology and geochemistry of Isla Floreana, Galápagos: A different type of late-stage ocean island volcanism. In K. S. Harpp, E. Mittelstaedt, N. d'Ozouville, & D. W. Graham (Eds.), *Geophysical Monograph series* (pp. 71–117). John Wiley & Sons, Inc. https://doi.org/10.1002/9781118852538.ch6

Harpp, K. S., Hall, P. S., & Jackson, M. G. (2014). Galápagos and easter: A tale of two hotspots. In K. S. Harpp, E. Mittelstaedt, N. d'Ozouville, & D. W. Graham (Eds.), *Geophysical Monograph series* (pp. 27–40). John Wiley & Sons, Inc. https://doi.org/10.1002/9781118852538.ch3

Harpp, K. S., & Weis, D. (2020). Insights into the origins and compositions of mantle plumes: A comparison of Galápagos and Hawai'i. *Geochemistry, Geophysics, Geosystems*, *21*. https://doi.org/10.1029/2019GC008887

Harpp, K. S., & White, W. M. (2001). Tracing a mantle plume: Isotopic and trace element variations of Galápagos seamounts. *Geochemistry, Geophysics, Geosystems*, *2*. https://doi.org/10.1029/2000gc000137

Harpp, K. S., Wirth, K. R., Teasdale, R., Blair, S., Reed, L., Barr, J., et al. (2014). Plume-ridge interaction in the Galápagos: Perspectives from Wolf, Darwin, and Genovesa Islands. In K. S. Harpp, E. Mittelstaedt, N. d'Ozouville, & D. W. Graham (Eds.), *Geophysical Monograph series* (pp. 285–334). John Wiley & Sons, Inc. https://doi.org/10.1002/9781118852538.ch15

Hart, S. R., Hauri, E. H., Oschmann, L. A., & Whitehead, J. A. (1992). Mantle plumes and entrainment: Isotopic evidence. *Science*, *256*, 517–520. https://doi.org/10.1126/science.256.5056.517

Hauri, E., Gaetani, G., & Green, T. (2006). Partitioning of water during melting of the Earth's upper mantle at H_2O-undersaturated conditions. *Earth and Planetary Science Letters*, *248*, 715–734. https://doi.org/10.1016/j.epsl.2006.06.014

Herzberg, C., & Asimow, P. D. (2008). Petrology of some oceanic island basalts: PRIMELT2.XLS software for primary magma calculation. *Geochemistry, Geophysics, Geosystems*, *9*. https://doi.org/10.1029/2008gc002057

Hirth, G., & Kohlstedt, D. (2003). Rheology of the upper mantle and the mantle wedge: A view from the experimentalists. In J. Eiler (Ed.), *Geophysical monograph series* (pp. 83–105). American Geophysical Union. https://doi.org/10.1029/138GM06

Hirth, G., & Kohlstedt, D. L. (1996). Water in the oceanic upper mantle: Implications for rheology, melt extraction and the evolution of the lithosphere. *Earth and Planetary Science Letters*, *144*, 93–108. https://doi.org/10.1016/0012-821X(96)00154-9

Hoernle, K., Werner, R., Morgan, J. P., Garbe-Schönberg, D., Bryce, J., & Mrazek, J. (2000). Existence of complex spatial zonation in the Galápagos plume. *Geology*, *28*, 4352–4438. https://doi.org/10.1130/0091-7613(2000)028<0435:eocszi>2.3.co;2

Hooft, E. E. E., Toomey, D. R., & Solomon, S. C. (2003). Anomalously thin transition zone beneath the Galápagos hotspot. *Earth and Planetary Science Letters*, *216*, 55–64. https://doi.org/10.1016/S0012-821X(03)00517-X

Iacovino, K., Matthews, S., Wieser, P., Moore, G., & Bégué, F. (2020). VESIcal part I: An open-source thermodynamic model engine for mixed volatile (H2O-CO2) solubility in silicate melts (preprint). *Earth Sciences*. https://doi.org/10.31223/X5D606

Ingle, S., Ito, G., Mahoney, J. J., Chazey, W., Sinton, J., Rotella, M., & Christie, D. M. (2010). Mechanisms of geochemical and geophysical variations along the western Galápagos Spreading Center. *Geochemistry, Geophysics, Geosystems*, *11*. https://doi.org/10.1029/2009gc002694

Ito, G., & Bianco, T. (2014). Patterns in Galápagos magmatism arising from the upper mantle dynamics of plume-ridge interaction. In K. S. Harpp, E. Mittelstaedt, N. d'Ozouville, & D. W. Graham (Eds.), *Geophysical monograph series* (pp. 245–261). John Wiley & Sons, Inc. https://doi.org/10.1002/9781118852538.ch13

Ito, G., & Lin, J. (1995). Oceanic spreading center–hotspot interactions: Constraints from along-isochron bathymetric and gravity anomalies. *Geology*, *23*, 6572. https://doi.org/10.1130/0091-7613(1995)023<0657:oschic>2.3.co;2

Ito, G., Lin, J., & Gable, C. W. (1997). Interaction of mantle plumes and migrating mid-ocean ridges: Implications for the Galápagos plume-ridge system. *Journal of Geophysical Research*, *102*, 15403–15417. https://doi.org/10.1029/97JB01049

Ito, G., Lin, J., & Graham, D. W. (2003). Observational and theoretical studies of the dynamics of mantle plume–mid-ocean ridge interaction. *Reviews of Geophysics*, *41*. https://doi.org/10.1029/2002RG000117

Ito, G., & Mahoney, J. J. (2005). Flow and melting of a heterogeneous mantle: 1. Method and importance to the geochemistry of ocean island and mid-ocean ridge basalts. *Earth and Planetary Science Letters*, *230*, 29–46. https://doi.org/10.1016/j.epsl.2004.10.035

Jackson, M. G., Koga, K. T., Price, A., Konter, J. G., Koppers, A. A. P., Finlayson, V. A., et al. (2015). Deeply dredged submarine HIMU glasses from the Tuvalu Islands, Polynesia: Implications for volatile budgets of recycled oceanic crust. *Geochemistry, Geophysics, Geosystems*, *16*, 3210–3234. https://doi.org/10.1002/2015GC005966

Jarosewich, E., Nelen, J. A., & Norberg, J. A. (1980). Reference samples for electron microprobe analysis. *Geostandards and Geoanalytical Research*, *4*, 43–47. https://doi.org/10.1111/j.1751-908X.1980.tb00273.x

Johnson, E. A. (2006). 6. Water in nominally anhydrous crustal minerals: Speciation, concentration, and geologic significance. In H. Keppler, & J. R. Smyth (Eds.), *Water in nominally anhydrous minerals* (pp. 117–154). De Gruyter. https://doi.org/10.1515/9781501509476-010

Katz, R. F., Spiegelman, M., & Langmuir, C. H. (2003). A new parameterization of hydrous mantle melting. *Geochemistry, Geophysics, Geosystems*, *4*. https://doi.org/10.1029/2002gc000433

Katz, R. F., & Weatherley, S. M. (2012). Consequences of mantle heterogeneity for melt extraction at mid-ocean ridges. *Earth and Planetary Science Letters*, *335–336*, 226–237. https://doi.org/10.1016/j.epsl.2012.04.042

Kelemen, P. B., Hirth, G., Shimizu, N., Spiegelman, M., & Dick, H. J. (1997). A review of melt migration processes in the adiabatically upwelling mantle beneath oceanic spreading ridges. *Philosophical Transactions of the Royal Society A: London Series, Mathematical Physical and Engineering Sciences*, *355*, 283–318. https://doi.org/10.1098/rsta.1997.0010

Keller, T., & Katz, R. F. (2016). The role of volatiles in reactive melt transport in the asthenosphere. *Journal of Petrology*, *57*, 1073–1108. https://doi.org/10.1093/petrology/egw030

Kendrick, M. A., Hémond, C., Kamenetsky, V. S., Danyushevsky, L., Devey, C. W., Rodemann, T., et al. (2017). Seawater cycled throughout Earth's mantle in partially serpentinized lithosphere. *Nature Geoscience*, *10*, 222–228. https://doi.org/10.1038/ngeo2902

Kendrick, M. A., Jackson, M. G., Hauri, E. H., & Phillips, D. (2015). The halogen (F, Cl, Br, I) and H_2O systematics of Samoan lavas: Assimilated-seawater, EM2 and high-$^3He/^4He$ components. *Earth and Planetary Science Letters*, *410*, 197–209. https://doi.org/10.1016/j.epsl.2014.11.026

Kingsley, R. H., & Schilling, J.-G. (1998). Plume-ridge interaction in the Easter-Salas y Gomez seamount chain-Easter Microplate system: Pb isotope evidence. *Journal of Geophysical Research*, *103*, 24159–24177. https://doi.org/10.1029/98JB01496

Kokfelt, T., Lundstrom, C., Hoernle, K., Hauff, F., & Werner, R. (2005). Plume-ridge interaction studied at the Galápagos spreading center: Evidence from ^{226}Ra-^{230}Th-^{238}U and ^{231}Pa-^{235}U isotopic disequilibria. *Earth and Planetary Science Letters*, *234*, 165–187. https://doi.org/10.1016/j.epsl.2005.02.031

Koleszar, A. M., Saal, A. E., Hauri, E. H., Nagle, A. N., Liang, Y., & Kurz, M. D. (2009). The volatile contents of the Galapagos plume; evidence for H_2O and F open system behavior in melt inclusions. *Earth and Planetary Science Letters*, *287*, 442–452. https://doi.org/10.1016/j.epsl.2009.08.029

Kurz, M. D., Curtice, J., Fornari, D., Geist, D., & Moreira, M. (2009). Primitive neon from the center of the Galápagos hotspot. *Earth and Planetary Science Letters*, *286*, 23–34. https://doi.org/10.1016/j.epsl.2009.06.008

Kurz, M. D., & Geist, D. (1999). Dynamics of the Galapagos hotspot from helium isotope geochemistry. *Geochimica et Cosmochimica Acta*, *63*, 4139–4156. https://doi.org/10.1016/S0016-7037(99)00314-2

Lambart, S. (2017). No direct contribution of recycled crust in Icelandic basalts. *Geochemical Perspectives Letters*, 7–12. https://doi.org/10.7185/geochemlet.1728

Langmuir, C. H., & Bender, J. F. (1984). The geochemistry of oceanic basalts in the vicinity of transform faults: Observations and implications. *Earth and Planetary Science Letters*, *69*, 107–127. https://doi.org/10.1016/0012-821X(84)90077-3

Le Roux, P., Shirey, S., Hauri, E., Perfit, M., & Bender, J. (2006). The effects of variable sources, processes and contaminants on the composition of northern EPR MORB (8–10°N and 12–14°N): Evidence from volatiles (H_2O, CO_2, S) and halogens (F, Cl). *Earth and Planetary Science Letters*, *251*, 209–231. https://doi.org/10.1016/j.epsl.2006.09.012

Le Voyer, M., Cottrell, E., Kelley, K. A., Brounce, M., & Hauri, E. H. (2015). The effect of primary versus secondary processes on the volatile content of MORB glasses: An example from the equatorial Mid-Atlantic Ridge (5°N–3°S): MORB volatile contents along 5°N–3°S MAR. *Journal of Geophysical Research: Solid Earth*, *120*, 125–144. https://doi.org/10.1002/2014JB011160

Le Voyer, M., Hauri, E. H., Cottrell, E., Kelley, K. A., Salters, V. J. M., Langmuir, C. H., et al. (2018). Carbon fluxes and primary magma CO_2 contents along the global mid-ocean ridge system. *Geochemistry, Geophysics, Geosystems*. https://doi.org/10.1029/2018GC007630

Maclennan, J., McKenzie, D., & Gronvöld, K. (2001). Plume-driven upwelling under central Iceland. *Earth and Planetary Science Letters*, *194*, 67–82. https://doi.org/10.1016/S0012-821X(01)00553-2

Marks, M. A. W., Kendrick, M. A., Eby, G. N., Zack, T., & Wenzel, T. (2017). The F, Cl, Br and I contents of reference glasses BHVO-2G, BIR-1G, BCR-2G, GSD-1G, GSE-1G, NIST SRM 610 and NIST SRM 612. *Geostandards and Geoanalytical Research*, *41*, 107–122. https://doi.org/10.1111/ggr.12128

Matthews, S., Shorttle, O., & Wong, K. (2020). *simonwmatthews/pyMelt*. Zenodo. https://doi.org/10.5281/ZENODO.4011814

Métrich, N., Zanon, V., Créon, L., Hildenbrand, A., Moreira, M., & Marques, F. O. (2014). Is the "Azores Hotspot" a Wetspot? Insights from the geochemistry of fluid and melt inclusions in Olivine of Pico Basalts. *Journal of Petrology*, *55*, 377–393. https://doi.org/10.1093/petrology/egt071

Michael, P. (1995). Regionally distinctive sources of depleted MORB: Evidence from trace elements and H2O. *Earth and Planetary Science Letters*, *131*, 301–320. https://doi.org/10.1016/0012-821X(95)00023-6

Michael, P. J. (1988). The concentration, behavior and storage of H_2O in the suboceanic upper mantle: Implications for mantle metasomatism. *Geochimica et Cosmochimica Acta*, *52*, 555–566. https://doi.org/10.1016/0016-7037(88)90110-X

Michael, P. J. (1999). Implications for magmatic processes at Ontong Java Plateau from volatile and major element contents of Cretaceous basalt glasses. *Geochemistry, Geophysics, Geosystems*, *1*. https://doi.org/10.1029/1999gc000025

Michael, P. J., & Cornell, W. C. (1998). Influence of spreading rate and magma supply on crystallization and assimilation beneath mid-ocean ridges: Evidence from chlorine and major element chemistry of mid-ocean ridge basalts. *Journal of Geophysical Research*, *103*, 18325–18356. https://doi.org/10.1029/98JB00791

Mittal, T., & Richards, M. A. (2017). Plume-ridge interaction via melt channelization at Galápagos and other near-ridge hotspot provinces. *Geochemistry, Geophysics, Geosystems*, *18*, 1711–1738. https://doi.org/10.1002/2016GC006454

Mittelstaedt, E., Soule, A. S., Harpp, K. S., & Fornari, D. (2014). Variations in crustal thickness, plate rigidity, and volcanic processes throughout the northern Galápagos Volcanic Province. In K. S. Harpp, E. Mittelstaedt, N. d'Ozouville, & D. W. Graham (Eds.), *Geophysical monograph series* (pp. 263–284). John Wiley & Sons, Inc. https://doi.org/10.1002/9781118852538.ch14

Morgan, W. J. (1971). Convection plumes in the lower mantle. *Nature*, *230*, 42–43. https://doi.org/10.1038/230042a0

Morgan, W. J. (1978). Rodriguez, Darwin, Amsterdam, ..., A second type of Hotspot Island. *Journal of Geophysical Research*, *83*, 5355. https://doi.org/10.1029/JB083iB11p05355

Peterson, M. E., Saal, A. E., Kurz, M. D., Hauri, E. H., Blusztajn, J. S., Harpp, K. S., et al. (2017). Submarine basaltic glasses from the Galapagos Archipelago: Determining the volatile budget of the mantle plume. *Journal of Petrology*, *58*, 1419–1450. https://doi.org/10.1093/petrology/egx059

Reekie, C. D. J., Jenner, F. E., Smythe, D. J., Hauri, E. H., Bullock, E. S., & Williams, H. M. (2019). Sulfide resorption during crustal ascent and degassing of oceanic plateau basalts. *Nature Communications*, *10*. https://doi.org/10.1038/s41467-018-08001-3

Ribe, N. M. (1996). The dynamics of plume-ridge interaction: 2. Off-ridge plumes. *Journal of Geophysical Research*, *101*, 16195–16204. https://doi.org/10.1029/96JB01187

Rosenthal, A., Hauri, E. H., & Hirschmann, M. M. (2015). Experimental determination of C, F, and H partitioning between mantle minerals and carbonated basalt, CO_2/Ba and CO_2/Nb systematics of partial melting, and the CO_2 contents of basaltic source regions. *Earth and Planetary Science Letters*, *412*, 77–87. https://doi.org/10.1016/j.epsl.2014.11.044

Ryan, W. B. F., Carbotte, S. M., Coplan, J. O., O'Hara, S., Melkonian, A., Arko, R., et al. (2009). Global multi-resolution topography synthesis. *Geochemistry, Geophysics, Geosystems*, *10*. https://doi.org/10.1029/2008gc002332

Saal, A. E., Hauri, E. H., Langmuir, C. H., & Perfit, M. R. (2002). Vapour undersaturation in primitive mid-ocean-ridge basalt and the volatile content of Earth's upper mantle. *Nature*, *419*, 451–455. https://doi.org/10.1038/nature01073

Salters, V. J. M., & Stracke, A. (2004). Composition of the depleted mantle. *Geochemistry, Geophysics, Geosystems*, *5*. https://doi.org/10.1029/2003gc000597

Schilling, J.-G. (1991). Fluxes and excess temperatures of mantle plumes inferred from their interaction with migrating mid-ocean ridges. *Nature*, *352*, 397–403. https://doi.org/10.1038/352397a0

Schilling, J.-G., Fontignie, D., Blichert-Toft, J., Kingsley, R., & Tomza, U. (2003). Pb-Hf-Nd-Sr isotope variations along the Galápagos Spreading Center (101°–83°W): Constraints on the dispersal of the Galápagos mantle plume. *Geochemistry, Geophysics, Geosystems*, *4*. https://doi.org/10.1029/2002GC000495

Schilling, J.-G., Kingsley, R. H., & Devine, J. D. (1982). Galapagos hot spot-spreading center system: 1. Spatial petrological and geochemical variations (83°W–101°W). *Journal of Geophysical Research*, *87*, 5593–5610. https://doi.org/10.1029/JB087iB07p05593

Shimizu, K., Ito, M., Chang, Q., Miyazaki, T., Ueki, K., Toyama, C., et al. (2019). Identifying volatile mantle trend with the water-fluorine-cerium systematics of basaltic glass. *Chemical Geology*, *522*, 283–294. https://doi.org/10.1016/j.chemgeo.2019.06.014

Shimizu, K., Saal, A. E., Myers, C. E., Nagle, A. N., Hauri, E. H., Forsyth, D. W., et al. (2016). Two-component mantle melting-mixing model for the generation of mid-ocean ridge basalts: Implications for the volatile content of the Pacific upper mantle. *Geochimica et Cosmochimica Acta*, *176*, 44–80. https://doi.org/10.1016/j.gca.2015.10.033

Shishkina, T. A., Botcharnikov, R. E., Holtz, F., Almeev, R. R., Jazwa, A. M., & Jakubiak, A. A. (2014). Compositional and pressure effects on the solubility of H_2O and CO_2 in mafic melts. *Chemical Geology*, *388*, 112–129. https://doi.org/10.1016/j.chemgeo.2014.09.001

Shishkina, T. A., Botcharnikov, R. E., Holtz, F., Almeev, R. R., & Portnyagin, M. V. (2010). Solubility of H_2O- and CO_2-bearing fluids in tholeiitic basalts at pressures up to 500 MPa. *Chemical Geology*, *277*, 115–125. https://doi.org/10.1016/j.chemgeo.2010.07.014

Shorttle, O., Maclennan, J., & Jones, S. M. (2010). Control of the symmetry of plume-ridge interaction by spreading ridge geometry. *Geochemistry, Geophysics, Geosystems*, *11*. https://doi.org/10.1029/2009gc002986

Sinton, J., Detrick, R., Canales, J. P., Ito, G., & Behn, M. (2003). Morphology and segmentation of the western Galápagos Spreading Center, 90.5°–98°W: Plume-ridge interaction at an intermediate spreading ridge. *Geochemistry, Geophysics, Geosystems*, *4*. https://doi.org/10.1029/2003GC000609

Sinton, J. M., & Detrick, R. S. (1992). Mid-ocean ridge magma chambers. *Journal of Geophysical Research*, *97*, 197. https://doi.org/10.1029/91JB02508

Sleep, N. H. (1990). Hotspots and mantle plumes: Some phenomenology. *Journal of Geophysical Research*, *95*, 6715. https://doi.org/10.1029/JB095iB05p06715

Sobolev, A. V., Hofmann, A. W., Kuzmin, D. V., Yaxley, G. M., Arndt, N. T., Chung, S.-L., et al. (2007). The amount of recycled crust in sources of mantle-derived melts. *Science*, *316*, 412–417.
Sorbadere, F., Médard, E., Laporte, D., & Schiano, P. (2013). Experimental melting of hydrous peridotite-pyroxenite mixed sources: Constraints on the genesis of silica-undersaturated magmas beneath volcanic arcs. *Earth and Planetary Science Letters*, *15*.
Stroncik, N. A., & Devey, C. W. (2011). Recycled gabbro signature in hotspot magmas unveiled by plume-ridge interactions. *Nature Geoscience*, *4*, 393–397. https://doi.org/10.1038/ngeo1121
Stroncik, N. A., Niedermann, S., & Haase, K. M. (2008). Plume-ridge interaction revisited: Evidence for melt mixing from He, Ne and Ar isotope and abundance systematics. *Earth and Planetary Science Letters*, *268*, 424–432. https://doi.org/10.1016/j.epsl.2008.01.037
Sun, Z., Xiong, X., Wang, J., Liu, X., Li, L., Ruan, M., et al. (2020). Sulfur abundance and heterogeneity in the MORB mantle estimated by copper partitioning and sulfur solubility modelling. *Earth and Planetary Science Letters*, *538*, 116169. https://doi.org/10.1016/j.epsl.2020.116169
Verma, S. P., & Schilling, J.-G. (1982). Galapagos hot spot-spreading center system: 2. $^{87}SR/^{86}SR$ and large ion lithophile element variations (85°W–101°W). *Journal of Geophysical Research: Solid Earth*, *87*, 10838–10856. https://doi.org/10.1029/JB087iB13p10838
Vidito, C., Herzberg, C., Gazel, E., Geist, D., & Harpp, K. (2013). Lithological structure of the Galápagos Plume: Lithological structure Galpagos Plume. *Geochemistry, Geophysics, Geosystems*, *14*, 4214–4240. https://doi.org/10.1002/ggge.20270
Villagómez, D. R., Toomey, D. R., Geist, D. J., Hooft, E. E. E., & Solomon, S. C. (2014). Mantle flow and multistage melting beneath the Galápagos hotspot revealed by seismic imaging. *Nature Geoscience*, *7*, 151–156. https://doi.org/10.1038/ngeo2062
Weatherley, S. M., & Katz, R. F. (2010). Plate-driven mantle dynamics and global patterns of mid-ocean ridge bathymetry. *Geochemistry, Geophysics, Geosystems*, *11*, n/a. https://doi.org/10.1029/2010gc003192
Weatherley, S. M., & Katz, R. F. (2012). Melting and channelized magmatic flow in chemically heterogeneous, upwelling mantle. *Geochemistry, Geophysics, Geosystems*, *13*. https://doi.org/10.1029/2011GC003989
Weis, D., Garcia, M. O., Rhodes, J. M., Jellinek, M., & Scoates, J. S. (2011). Role of the deep mantle in generating the compositional asymmetry of the Hawaiian mantle plume. *Nature Geoscience*, *4*, 831–838. https://doi.org/10.1038/ngeo1328
White, W. M., & Hofmann, A. W. (1978). *Geochemistry of the Galápagos islands: Implications for mantle dynamics and evolution* (Vol. *77*, pp. 596–606). Year Book Carnegie Inst. Washington.
White, W. M., McBirney, A. R., & Duncan, R. A. (1993). Petrology and geochemistry of the Galápagos Islands: Portrait of a pathological mantle plume. *Journal of Geophysical Research*, *98*, 19533–19563. https://doi.org/10.1029/93JB02018
Wieser, P. E., Jenner, F., Edmonds, M., Maclennan, J., & Kunz, B. E. (2020). Chalcophile elements track the fate of sulfur at Kīlauea Volcano, Hawai'i. *Geochimica et Cosmochimica Acta*, *282*, 245–275. https://doi.org/10.1016/j.gca.2020.05.018
Workman, R. K., & Hart, S. R. (2005). Major and trace element composition of the depleted MORB mantle (DMM). *Earth and Planetary Science Letters*, *231*, 53–72. https://doi.org/10.1016/j.epsl.2004.12.005
Workman, R. K., Hauri, E., Hart, S. R., Wang, J., & Blusztajn, J. (2006). Volatile and trace elements in basaltic glasses from Samoa: Implications for water distribution in the mantle. *Earth and Planetary Science Letters*, *241*, 932–951. https://doi.org/10.1016/j.epsl.2005.10.028

References From the Supporting Information

Connolly, J. (2009). The geodynamic equation of state: What and how. *Geochemistry, Geophysics, Geosystems*, *10*(10).
Hanyu, T., Shimizu, K., Ushikubo, T., Kimura, J.-I., Chang, Q., Hamada, M., & Ishikawa, T. (2019). Tiny droplets of ocean island basalts unveil Earth's deep chlorine cycle. *Nature Communications*, *10*(1), 60.
Holland, T. J., Green, E. C., & Powell, R. (2018). Melting of peridotites through to granites: A simple thermodynamic model in the system KNCFMASHTOCr. *Journal of Petrology*, *59*(5), 881–900.
Jennings, E. S., & Holland, T. J. (2015). A simple thermodynamic model for melting of peridotite in the system NCFMASOCr. *Journal of Petrology*, *56*(5), 869–892.
Kendrick, M. A., Jackson, M. G., Kent, A. J., Hauri, E. H., Wallace, P. J., & Woodhead, J. (2014). Contrasting behaviours of CO_2, S, H_2O and halogens (F, Cl, Br, and I) in enriched-mantle melts from Pitcairn and Society seamounts. *Chemical Geology*, *370*, 69–81.
Matthews, S., Wong, K., Shorttle, O., Edmonds, M., & Maclennan, J. (2021). Do olivine crystallization temperatures faithfully record mantle temperature variability? *Geochemistry, Geophysics, Geosystems*, *22*(4), e2020GC009157.
Miller, W. G., Maclennan, J., Shorttle, O., Gaetani, G. A., Le Roux, V., & Klein, F. (2019). Estimating the carbon content of the deep mantle with Icelandic melt inclusions. *Earth and Planetary Science Letters*, *523*.
Rudge, J. F., Maclennan, J., & Stracke, A. (2013). The geochemical consequences of mixing melts from a heterogeneous mantle. *Geochimica et Cosmochimica Acta*, *114*, 112–143.